Geophys. J. Int. (2006) **167,** 1385–1401 doi: 10.1111/j.1365-246X.2006.03144.x

Geophysical constraints on the crustal architecture of the Troodos ophiolite: results from the IANGASS project

G. D. Mackenzie,[1,*] P. K. H. Maguire,[1] L. A. Coogan,[2] M. A. Khan,[1] M. Eaton[1,†] and G. Petrides[3]

[1] *Department of Geology, University of Leicester, Leicester LE1 7RH, UK. E-mail: gmackenzie@cgg.com*
[2] *School of Earth and Ocean Sciences, University of Victoria, BC, Canada*
[3] *Cyprus Geological Survey, Nicosia, Cyprus*

Accepted 2006 July 15. Received 2006 July 4; in original form 2005 November 22

SUMMARY

We present results from modelling a combined 160 km seismic wide-angle reflection/refraction and gravity profile sited across the sheeted dykes, lavas and sediments of the northern part of the Troodos ophiolite, Cyprus. The *P*-wave seismic velocity and density model, including five separate layers, is defined to a depth of ∼10 km. This shows the ophiolite sequence dipping to the east beneath the central, well resolved, 85 km section of the line between Kambos in the west and Kelia in the east. The upper layer (average velocity 2.83 km s^{-1}; density 2.21 g cm^{-3}) is interpreted as consisting of sediments and the upper extrusive group. Beneath this, accepting that layer boundaries may be gradational beyond the experiment resolution, the layers are identified as the lower extrusive and basal groups (3.57 km s^{-1}; 2.31 g cm^{-3}), the sheeted dyke complex (SDC) (4.57 km s^{-1}; 2.72 g cm^{-3}), a gabbroic layer (6.31 km s^{-1}; 2.92 g cm^{-3}), and an ultramafic cumulate layer and/or serpentinized peridotite (7.00 km s^{-1}; 3.00 g cm^{-3}). While the thickness (∼6 km) of this layer beneath the proposed gabbroic layer is defined, positive identification of its composition is not possible, owing to the lack of discriminatory *S*-wave velocity information. The underlying material provides an unreversed velocity of 8.0 km s^{-1} beneath the western end of the profile. These modelled velocities and densities are compared with seismic models of oceanic crust and their implications for models of the tectonic evolution of the Troodos ophiolite are discussed.

Several major faults are interpreted from the models, with throws of up to ∼500 m offsetting both the extrusive-SDC and the SDC-gabbroic layer boundaries. These are all downthrown to the west, there being no evidence from the data to suggest any major faults downthrown to the east. Our results therefore do not support existing tectonic models for a multiple graben structure within the ophiolite recording either the progress of an eastward stepping spreading centre or off-axis graben formation. Instead, assuming that the faults are downthrown towards the ridge axis, the data are consistent with a single spreading centre located to the west of the recording profile.

Key words: Cyprus, oceanic crustal structure, seismic wide-angle reflection/gravity profile, Troodos ophiolite.

INTRODUCTION

The Troodos ophiolite is one of the best studied ophiolites in the world and has played a pivotal role in the development of concepts concerning the process of seafloor spreading (e.g. Robertson & Xenophontos 1993). However, despite extensive investigations, the role of tectonic extension and graben formation in the architecture of the Troodos oceanic crust are still unclear. Also crustal layer thickness and the nature of the underlying mantle, both of which have significant implication concerning the formation conditions of this supra-subduction zone oceanic crust, are poorly known. This is largely because geological studies have been carried out using imperfect exposures with relatively little vertical control. To overcome many of these problems the Investigations Around North Troodos using Gravity And Seismic Surveys (IANGASS) geophysical survey was conducted in 1995. This consisted of a coincident wide-angle

[*] Now at: Compagnie Generale de Geophysique, c/o BP Exploration Aberdeen, Farburn Industrial Estate, Dyce, Aberdeen, AB21 7PB, UK.
[†] Now at: PGS Marine Geophysical, Strandveien 4, N-1326 Lysaker, Norway.

reflection/refraction seismic and gravity profile across the sheeted dykes, extrusives and sediments of the northern part of the Troodos ophiolite complex, with the following original objectives:

(1) To investigate the internal architecture of the upper crust, to determine crustal thickness and to examine the upper mantle structure beneath the ophiolite.

(2) To delineate the structure of three proposed grabens [the Solea, Mitsero and Larnaca graben] and comment on their interpretation as spreading centres.

(3) To test existing models for the origin of tectonic extension in the sheeted dyke complex and to investigate whether this is rooted in a detachment at the dyke-gabbro transition or whether faults penetrate this boundary.

TECTONIC AND GEOLOGICAL BACKGROUND

The Troodos ophiolite formed in a supra-subduction zone setting (Miyashiro 1973) in the Late Cretaceous (*ca*. 91 Ma; Mukasa & Ludden 1987). It is exposed over a large area (Fig. 1) and has an overall domal geometry centred on Mt Olympus. The core of the dome is serpentinized mantle peridotite; this is surrounded by a plutonic then a sheeted dyke complex (SDC) with overlying extrusive lavas and sediments. The lava sequence has been divided, based on field characteristics and geochemistry, into an upper and a lower sequence (Wilson 1959; Gass 1960). The sheeted dyke complex, which is excellently exposed, consists of generally north–south trending dykes indicating east–west spreading in the present geographic framework. A gradational 'basal' or transitional layer (e.g. Bear 1960) comprised of a variable proportion of dykes and lavas has been identified above the sheeted dyke complex. The underlying plutonics are less well exposed than the sheeted dykes. They are characterized by a complex mixture of felsic, mafic and ultramafic cumulates. There is no consistent distribution of these lithologies with depth in the crust although there are greater proportions of felsic intrusions at shallow levels and ultramafic intrusions at depth.

Many aspects of the post-formation history of the Troodos ophiolite are controversial. A simplified model can be summarized as follows.

Palaeomagnetic studies show that the Troodos ophiolite has rotated *ca*. 90° anticlockwise since its formation with most of this rotation occurring before the end of the Early Eocene (within 40 Myr of ophiolite formation) (e.g. Clube *et al.* 1985). The sedimentary succession overlying the ophiolite shows that this rotation was followed by periods of compression and uplift forming the dome-like structure and leading to emergence of the Troodos oceanic crust above sea level. Robertson (1998) suggests the unbroken sedimentary cover through the Late Cretaceous into the Tertiary rules out the classical model in which the ophiolite was emplaced by long-distance thrusting onto the Arabian continental margin in the Late Cretaceous (e.g. Dercourt *et al.* 1993). Instead, he surmises the

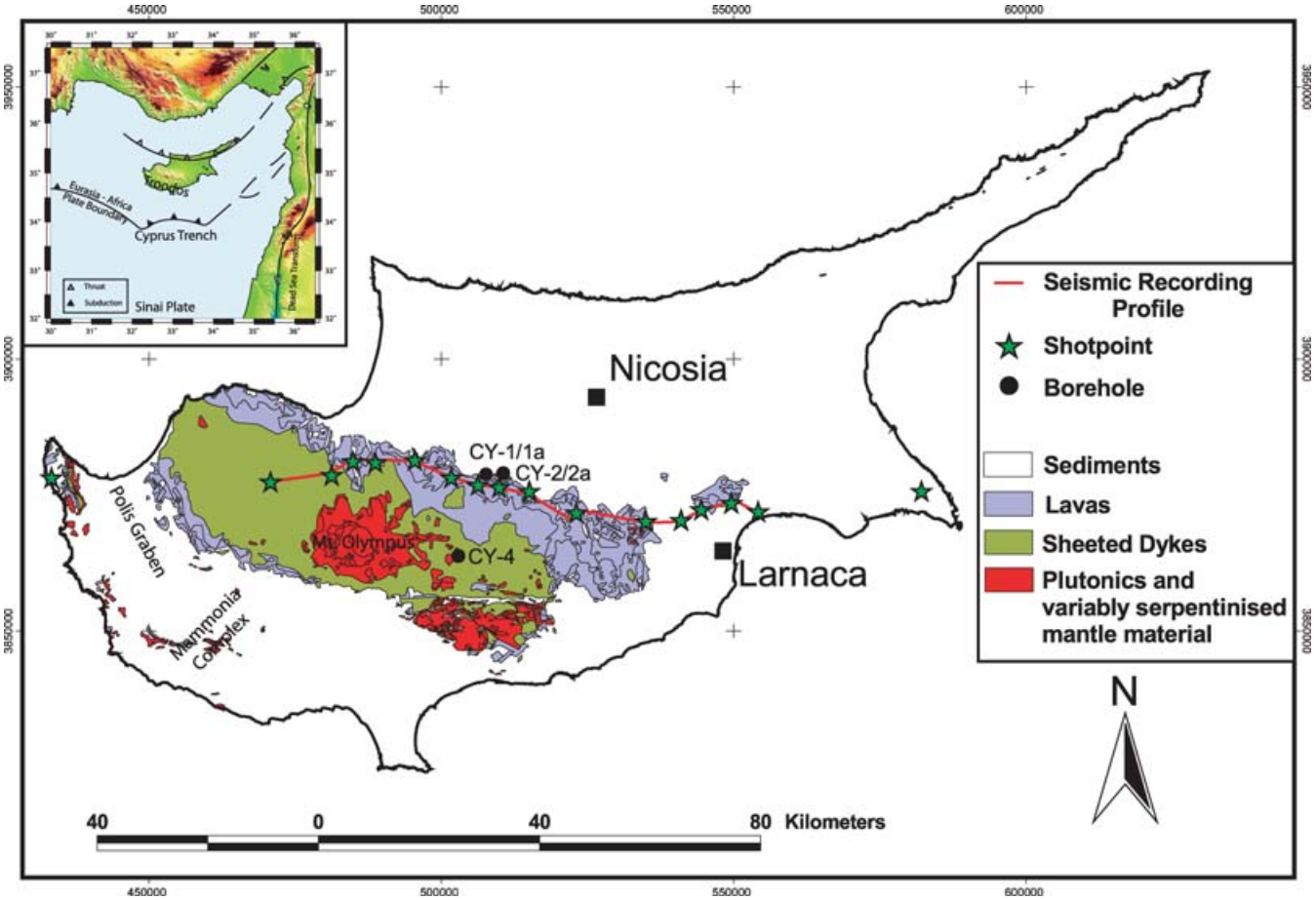

Figure 1. Simplified geological map of the Troodos ophiolite (based on maps from the Geological Survey of Cyprus). Inset shows the tectonic setting of the region (after Robertson 1998). The location of the IANGASS geophysical profile is indicated by the red line. CY-n identify the locations of the Cyprus Crustal Study Project (CCSP) boreholes (Salisbury *et al.* 1989). WGS 84 UTM location zone 36N.

ophiolite remained within a remnant of the Neotethyan ocean during the Tertiary, and was then uplifted in the Pliocene and Pleistocene, with most uplift occurring in the Late Pliocene to mid-Pleistocene (Poole & Robertson 1992). The central portion of the ophiolite, around Mt Olympus was uplifted rapidly, probably due to the upward motion of a deep serpentinite diapir, now exposed at the surface. He adds that the impingment of the Eratosthenes seamount on the Cyprus trench during ongoing subduction to the south of the island, was also important in the upwarping of the Troodos ophiolite. Compositional studies suggest that the mantle section of the ophiolite can be divided into a partially serpentinized (*ca*. 40 per cent) harzburgite formed as a residue of melting to form the ophiolite crust and an almost totally serpentinized core that has been juxtaposed with the ophiolite by these later tectonic movements (e.g. Batanova & Sobolev 2000).

The present-day Cyprus-trench (Fig. 1), along which the Sinai microplate is subducted beneath Cyprus, lies *ca*. 50 km south of the island (e.g. Mascle *et al.* 2000). Weak and diffuse seismicity beneath Cyprus indicates that subduction may now have virtually ceased along the Cyprus Arc (Kempler & Ben-Avraham 1987) and that the margin is in transition from subduction to collision (Robertson 1998). To the west of the Troodos complex lies the Polis graben, a late Miocene basin located in a region of inferred supra-subduction zone extension (e.g. Payne & Robertson 1995).

MODELS FOR THE SPREADING EVOLUTION OF THE TROODOS CRUST

A number of studies have proposed a relatively simple spreading history for the Troodos ophiolite. Kidd & Cann (1974) showed that there is a slight preference for dykes to show eastern side chilled margins over western side chills implying that the ophiolite formed at a spreading centre to the west of the ophiolite. A subsequent study by Baragar *et al.* (1990) also found that on average, east side chills are more abundant but suggested that this was not statistically significant. Ages of the oldest sediment overlying the ophiolite, based on limited radiolarian ages, lend some support to a spreading centre to the west of the ophiolite (Osozawa & Okamura 1993); however, these data are too limited to be conclusive. A simple spreading history has also been proposed based on the relatively thin transition between the sheeted dyke and lava complexes which suggests that most dykes were intruded in a relatively narrow zone at the ridge axis (Cann 1970, 1974).

A more complex spreading history for the ophiolite has been suggested from the study of dyke orientations, along with paleomagnetic studies of dyke rotations. Varga & Moores (1985) proposed that the geometry of dykes within the SDC defines three approximately north–south trending grabens with dykes dipping inwards on each of their flanks. These were interpreted as fossil spreading centres. Cross-cutting relationships within the SDC led them to suggest that the oldest spreading centre was located in the vicinity of Solea and the youngest close to Larnaca with an intermediate-age spreading centre located between these two near Mitsero (Fig. 2a). At least two of the proposed grabens (Solea and Mitsero) are asymmetric with broader western sides (defined by eastward-dipping dykes) than eastern sides (defined by westward-dipping dykes). They note that the sediments overlying the ophiolite are only slightly deformed and dip gently to the north, which requires dyke rotation prior to sediment deposition. However, palaeomagnetic studies show that dykes were rotated after high-temperature (*ca*. 300°C) alteration (Varga *et al.* 1999). Varga & Moores (1985) propose that the dyke rotations root into a basal detachment, such as the Kakopetria detachment beneath the Solea graben where subhorizontal dykes overlie plutonic rocks.

This picture of three fossil spreading centres has been questioned. Allerton & Vine (1987) suggest that the large areas of the ophiolite that display a simple internal structure, including near-vertical dykes, and the subdued topography on the lava-sediment interface, support a simpler mode of accretion. In 1991 they suggested that spreading originated in the vicinity of the present Solea graben, the Mitsero graben resulting from off-axis tectonic extension to the east of the ridge axis. The spreading ridge then jumped to the east to the vicinity of the present Larnaca graben. There followed a period of largely amagmatic stretching which formed the structures that now define the Solea graben. Allerton & Vine (1991) suggest that the Larnaca graben itself may be analagous to the Solea graben, forming in a discrete stretching event, which may or may not be associated with the later abandonment of the new ridge in the present Larnaca graben. In a detailed study of dyke orientations Van Everdingen & Cawood (1995) show that there are many domains of apparently consistent dyke orientations that do not necessarily fit the simple three graben model. Furthermore, the detachment fault near the base of the sheeted dyke complex described in the Solea area (Varga & Moores 1985) is clearly absent in other areas.

Alternative models for deformation partitioning within the oceanic crust have been proposed based on the Troodos ophiolite. Agar & Klitgord (1995) suggested that deformation is decoupled between the sheeted dyke complex and the plutonic complex based largely on the observation that dykes and faults in the plutonic complex dip west while they dip east in the sheeted dyke complex. However, Coogan *et al.* (2002) show that many of the dykes intruding the plutonics are more depleted in incompatible trace elements than those in the sheeted dyke complex. This suggests that they may not have all been intruded as vertical parallel sheets at the same time, followed by differential rotation as required by Agar & Klitgord (1995). Other models suggest decoupling between the deformation in the lavas and sheeted dyke complex, incorporating two phases of lava rotation (e.g. Schouten & Denham 2000).

The IANGASS project was designed to examine the internal architecture of the Troodos crust as well as to sample the immediate upper mantle. Identification of faults cross-cutting the ophiolite layers was intended to throw light on the validity of the various models described above.

PREVIOUS GEOPHYSICAL STUDIES

While there have been several seismic surveys offshore Cyprus (e.g. Makris *et al.* 1983; Ben-Avraham *et al.* 1995) onshore geophysical studies of the Troodos Ophiolite have been primarily based on gravity surveys. Gass & Masson-Smith (1963) interpeted such surveys conducted in 1946 and 1958 and proposed a cone shaped low density granitic boss, or a diapirically emplaced serpentine body, to explain a localized circular negative anomaly concident with the summit of Mt Olympus. A detailed gravity survey of the Mt Olympus region itself was conducted by Shelton (1993). The results were explained in terms of a fully serpentinized mantle body of less than 10 km in diameter extending to an average depth of 15 km within altered depleted mantle. Shelton (1993) modelled a Moho thinning from 10 km depth beneath the southern coast of Cyprus to outcrop on Mt Olympus and then deepening to 4 km depth 30 km to the north of Mt Olympus. Makris *et al.* (1983) conducted a N–S seismic refraction survey between Israel and Cyprus, incorporating nine

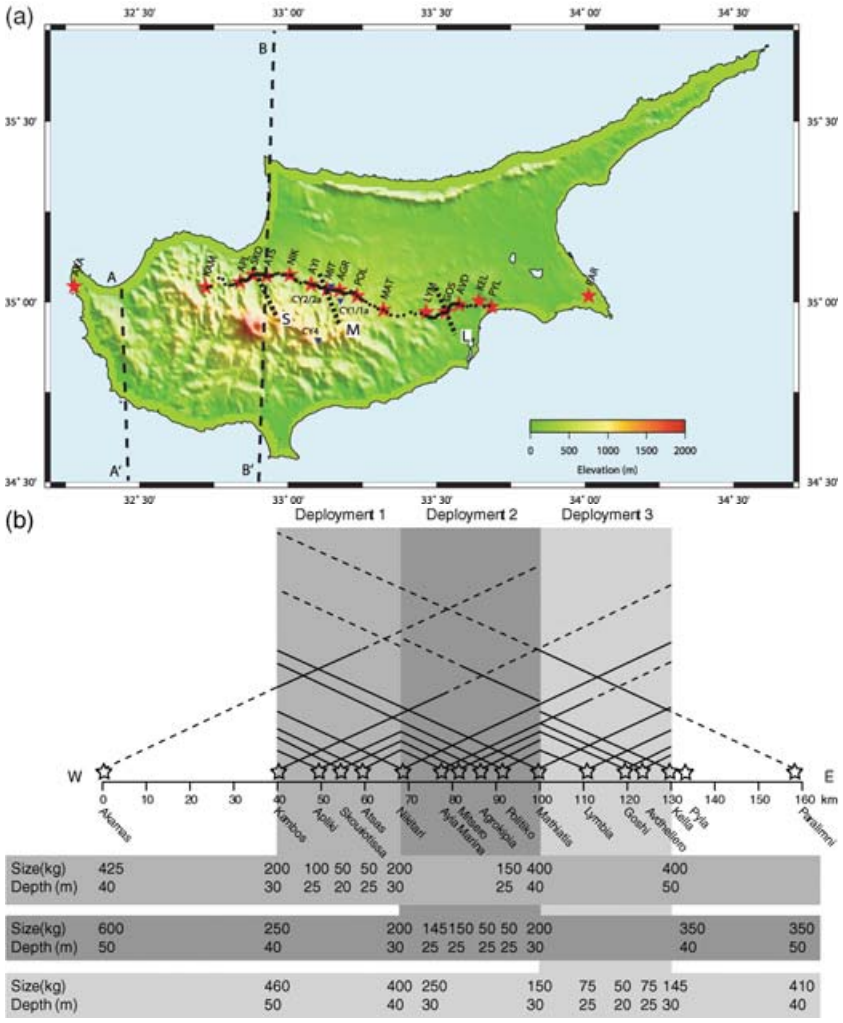

Figure 2. (a) Topographic map of Cyprus showing the location of IANGASS 1995 geophysical survey. Shotpoints are indicated by the red stars, seismic instruments by the black dots. The gravity survey was coincident with the seismic profile. Location of the CCSP boreholes (Salisbury *et al.* 1989) mentioned in the text are indicated by the inverted blue triangles. Shotpoint labels: AKA, Akamas; KAM, Kambos; APL, Apliki; SKO, Skouriotissa; ATS, Atsas; NIK, Nikitari; AYI, Ayia Marina; MIT, Mitsero; AGR, Agrokipia; POL, Politiko ; MAT, Mathiatis; LYM, Lymbia; GOS, Goshi; AVD, Avdhellero; KEL, Kelia; PYL, Pyla; PAR, Paralimni. The previously proposed locations of the Solea (S), Mitsero (M) and Larnaca (L) grabens are shown between shotpoints APL and ATS, shotpoints AYI and POL, and shotpoints LYM and AVD, respectively. The Khan *et al.* (1972) seismic survey was located between shotpoints SKO and MIT. The locations of the seismic profile of Makris *et al.* (1983) and gravity profile of Ergün *et al.* (2005) are indicated by the dashed lines A-A′ and B-B′ respectively. (b) Observation scheme for the seismic survey showing details of the three deployments. The solid lines show the distance to which significant energy was observed, while the dashed lines show the range to which recording was undertaken for the particular shots. No recordings were undertaken for the long offset shots from Akamas to Kambos and from Paralimni to Kelia. Also shown are the shot sizes and hole depths.

onshore stations within the Polis graben in western Cyprus to the west of the ophiolite (Fig. 2a). They modelled a 35-km-thick 'continental crust' beneath this part of their profile, thinning southwards. As ray coverage was poor beneath Cyprus their model was partially constrained using gravity data. Ergün *et al.* (2005) modelled four gravity profiles across the Cyprus arc, one near north–south crossing the Eratosthenes seamount and the Troodos ophiolite (Fig. 2a). This was interpreted in terms of thick sediments over the plate boundary suture with thinned continental crust beneath the Eratosthenes seamount to the south. The gravity high on Cyprus was interpreted as being caused by a combination of the Troodos ophiolite (modelled as an ∼2 km thick body of density 3.0 g cm^{-3}, thinner than suggested by geological studies) and a thinning of the sedimentary section above continental crust that is thinner (20 km) than that suggested by Makris *et al.* (1983) to the west of the Troodos ophiolite.

Khan *et al.* (1972) conducted a ∼20 km long seismic refraction survey along the northern margin of the ophiolite between Skouriotissa (SKO) and Mitsero (MIT) (Fig. 2a), obtaining a three layered crustal model using the plus-minus method of interpretation (Hagedoorn 1959). The model was interpreted in terms of a thin (0.5 km) layer of mean velocity 3.25 km s^{-1} interpreted as pillow lavas, above a basal layer with velocity approximately 5.2 km s^{-1}, overlying a layer of velocity 6.38 km s^{-1} at a depth of about 1.5–2.0 km, thought to be the 'diabase' or sheeted dyke unit. Lort & Matthews (1972) shot 16 short (200–1300 m) seismic profiles, each confined to a single constituent rock type of the ophiolite complex, to determine velocities within that lithology. Velocities were again calculated using the plus-minus method of Hagedoorn (1959). The objective was to compare the velocities with those of oceanic crust obtained from marine refraction profiles. However, the velocities obtained were

lower than expected with velocities ranging from 2.8 km s^{-1} in the pillow lavas to 5.5 km s^{-1} in the gabbros and only 3.8 km s^{-1} in the ultramafic rocks. The relatively low velocities were attributed to the high fracturing and alteration of the Troodos rocks. A principal outcome was the suggestion that the boundary between oceanic seismic layer 2 and layer 3 may represent a reduction in bulk porosity from the closure of cracks by overburden pressure rather than a petrological or metamorphic boundary. More recent studies around deep Ocean Drilling Program (ODP) drill holes have confirmed that this seismic boundary does not simply correlate with a lithological boundary as discussed in detail below. Both the Lort & Matthews (1972) and Khan *et al.* (1972) profiles were too short to sample deeper layers.

A survey including four nominal 12 km seismic refraction profiles in the vicinity of Mathiatis (MAT, Fig. 2a) resulted in a model of sediments and the upper extrusive layer (V_P 2.2–2.7 km s^{-1}) overlying the lower extrusive layer and basal group (V_P 3.1–4.3 km s^{-1}) above the sheeted dyke complex (V_P 5.1–5.5 km s^{-1}) (Cooper 1993).

In the late 1980s the Cyprus Crustal Study Project (CCSP) drilled a series of holes (Figs 1 and 2a) designed to sample the complete ophiolite sequence. Downhole logging in CY-4 and a number of previously drilled shallow holes provided velocity, density and electrical properties for the ophiolite sequence (Salisbury *et al.* 1989) (see Table 4). Velocities of 3.2–3.5 km s^{-1} were obtained in the extrusive lavas, 5–6.4 km s^{-1} in the SDC and 6.7–6.9 km s^{-1} in the gabbros. Velocities of 7–7.4 km s^{-1} were logged in the underlying pyroxenites. Laboratory measurements on samples from CY-1 (Smith & Vine 1991), CY-2 (Smith & Vine 1987) and CY-4 (Smith & Vine 1989) provided a range of values for the lavas (which included both highly altered and fresh flows and intrusives) averaging at ∼3.5 km s^{-1}. Velocities averaged ∼4.8 km s^{-1} in the sheeted dykes in CY-1, 1a, 2 and 2a, and ∼6.5 km s^{-1} in CY-4. In CY-4 the average velocity for the gabbro was 6.93 km s^{-1} and for the ultramafics was 7.26 km s^{-1}, being equivalent to the logged velocities. In CY-4 logged densities increase from 2.2 to 2.3 g cm^{-3} in the pillow lavas to 2.6–2.8 g cm^{-3} in the dykes, 2.9–2.95 g cm^{-3} in the gabbros and 3.1 g cm^{-3} in the ultramafics (Salisbury *et al.* 1989) being equivalent to those identified from the laboratory measurements of Smith & Vine (1987, 1989, 1991). In general the logged formation velocity and densities were found to be lower than those of the rock samples primarily due to the effects of porosity and anisotropy (Salisbury *et al.* 1989).

THE IANGASS 1995 PROJECT

The IANGASS 1995 project involved the joint acquisition of a wide-angle seismic reflection/refraction and coincident gravity profile across the Troodos Ophiolite complex, extending from near the centre of the ophiolite eastwards into the circum-Troodos sedimentary succession (Figs 1 and 2). Gravity measurements were made at 239 stations located along the length of the IANGASS seismic profile from AKA to PAR (Fig. 2). A local gravity network of 19 base stations was established and linked to a gravity reference station at Malounda, near the centre of the profile. The roving station measurements were taken in loops, starting and ending at a base station, to enable correction for instrument drift.

The acquisition of the wide-angle reflection/refraction profile was conducted in three deployments (Fig. 2b) during the spring of 1995. Over the three deployments a total of 196 seismic stations recorded up to 29 shots of between 50 and 600 kg. Station spacing was variable with a denser nominal 250 m spacing across the proposed spreading centres (the Solea, Mitsero and Larnaca grabens). The seismic instrumentation used for the survey consisted of a combination of Teledyne PDAS 100 and Reftek 72A digital recorders connected, for the most part, to vertical component 4.5 Hz geophones. The dense station spacing within the centre of each deployment was obtained by connecting vertical component geophones to all three channels of each recorder, two being deployed at the end of 250 m cables. A small number of instruments were kept fixed throughout the entire survey to provide reciprocal times for long offset recordings and duplicate recordings for quality control. These were mostly three component Willmore 1 Hz seismometers. Site locations were derived from GPS receivers. The majority of the sites had permanent GPS antennae synchronizing the recorders internal time signal every 60 min while the remainder had their internal clocks synchronized daily to GPS time by field crews. Time corrections for clock drift were calculated and applied to each seismic trace individually.

DATA MODELLING

Seismic modelling

Section description and phase picking

The complete seismic data set has been combined into shot-gathers, converted into SEGY format, corrected for the time drift of the internal clocks and displayed using ZP, an interactive plotting and picking software package (B. Zelt, personal communication, 2003). Example vertical component seismic sections are shown in Figs 3(a–d). While increasing the station density over the central section of each deployment, the use of a large number of cables for the recordings also resulted in higher noise levels. The experiment was undertaken at a time when severe distant electrical storms occurred resulting in significant electrical induction with signals being recorded by the cables, these being in effect a 500 m 'ground aerial' deployed from many of the recorders. While the raw data set displayed a clear seismic structure, the resulting filtered signals showed severe ringing with a dominant frequency of the order of 12–18 Hz (Figs 3a–d). However, the principal phases of interest (first arrivals and a number of second arrivals correlated over significant distances) are clearly visible on the resultant sections. Possibly because of the severe electrical noise, the identification of shear-wave energy has proved extremely difficult. The small number of three-component seismometers did not prove sufficient to provide confidence in *S*-phase identification on the vertical component recordings.

Despite the difficulties with data acquisition, we consider the *P*-wave data quality to be good with first arrival energy propagation dependent on charge size but observed to ∼90 km offset for the largest charges (Fig. 3d). The sections all show first arrivals with high apparent velocities (>5 km s^{-1}) at only ∼5 km offset. Several strong reflectors are visible with a deep reflector observed to ∼120 km from shotpoint PAR (Fig. 3d). To aid the identification of traveltime phases, traveltime reciprocity was checked where possible (Zelt 1999). Traveltimes were picked using ZP, the picks being assigned an error (Table 1) based on the signal to noise ratio of the data within a 0.25 s time window around the traveltime pick. This picking error was then used to weight the traveltimes during the inversion procedure.

Seismic tomography

Modelling of the IANGASS 1995 wide-angle seismic data set was conducted using both a minimum structure tomographic approach

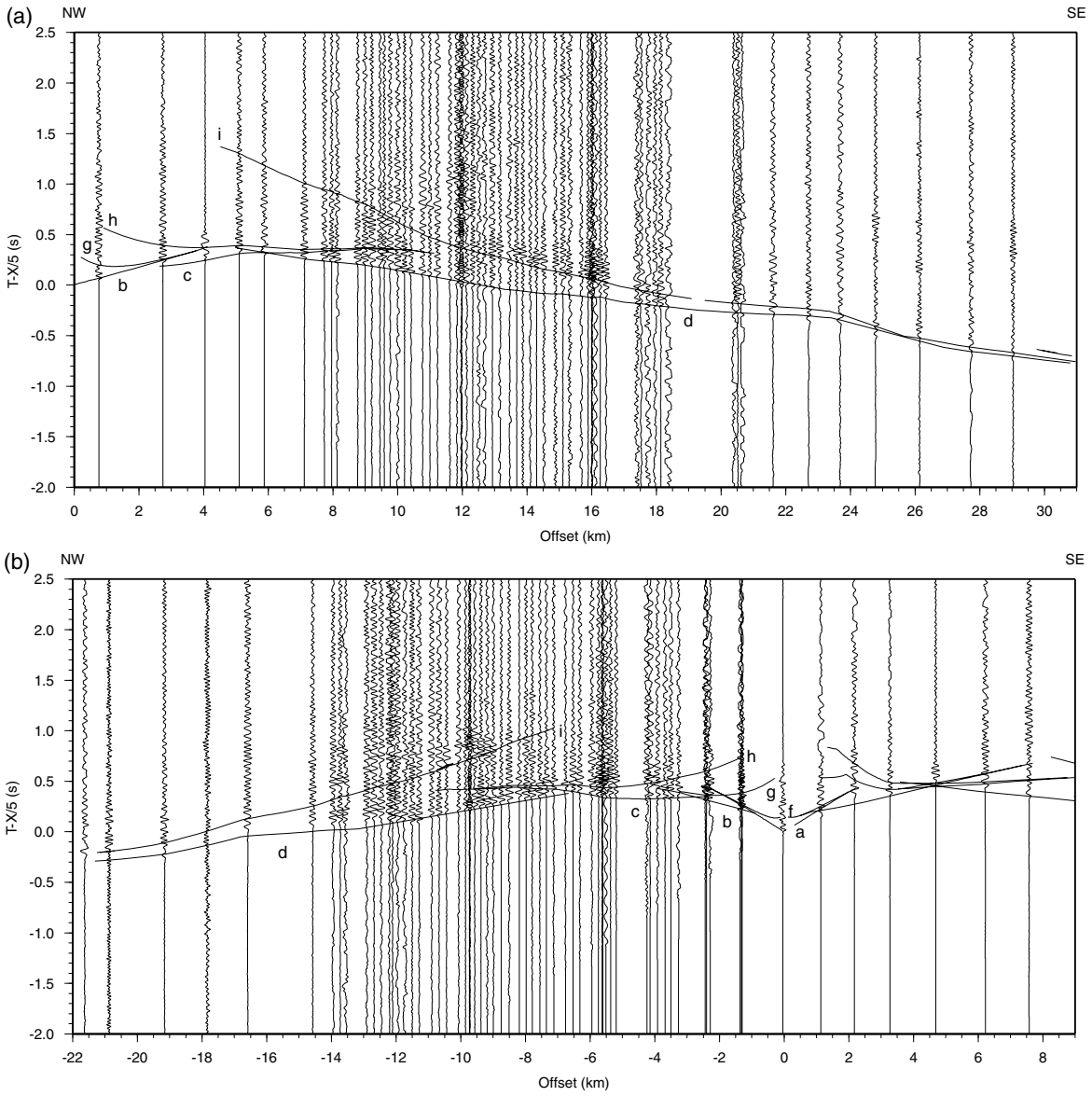

Figure 3. Processed seismic sections bandpass filtered from 0.5 to 30 Hz with modelled traveltimes overlain. For clarity only every second trace has been plotted in the regions of dense station spacing. Phase labels: (a) refraction in the sediments; (b) refraction in the volcanics; (c) refraction in the SDC; (d) refraction in the gabbroic layer; (e) refraction in the ultramafics or plutonics; (f) reflection from the base of the sediments;(g) reflection from the base of the volcanics; (h) reflection from the base of the SDC; (i) reflection from the base of the gabbroic layer; (j) reflection from the base of the ultramafic/plutonic layer. Panel (a) from shotpoint NIK into deployment 2 reduced at 5 km s^{-1}. Panel (b) from shotpoint POL into deployment 2 reduced at 5 km s^{-1}. Panel (c) from shotpoint MAT into the entire profile reduced at 6 km s^{-1}. Panel (d) from shotpoint PAR at the eastern end of the entire profile, reduced at 6 km s^{-1} and bandpass filtered from 2 to 20 Hz. Arrows in panel (d) indicate a reflector with a traveltime >3 s behind the first arrivals.

and a more traditional ray tracing technique. The first arrival seismic tomography (FAST) regularized inversion algorithm (Zelt & Barton 1998) was used to create a 2-D tomographic model beneath the best-fit line through the whole IANGASS profile using the picked first arrival traveltimes. The software utilizes a regularized inversion with a combination of smallest, flattest and smoothest perturbation constraints which are specified by the user. The inversion uses a least squares variation of the conjugate gradient technique. The algorithm automatically tests a number of damping values (λ) during each iteration to assess which gives the best solution. This solution is a trade off between minimizing the agreement of the model to the data and the smoothness or stability of the solution. The starting model was taken to be a simple 1-D model which was firstly inverted with no damping. However, a smoothing filter was applied to the model after each iteration to allow the long wavelength features to be derived. This smoothed 2-D model was then used as a starting model for a second run of the inversion routine where a variety of damping values were tested at each iteration to produce a final model (Fig. 4).

The seismic tomography model

The resulting final model (Fig. 4) shows high velocities of >6 km s^{-1} at relatively shallow depths across the main section of the profile (KAM–KEL_PYL) with a very high velocity body (>7 km s^{-1}) at 4 km depth between shotpoints KAM and AYI, shallowing between NIK and AYI. In general the velocity contours suggest the high

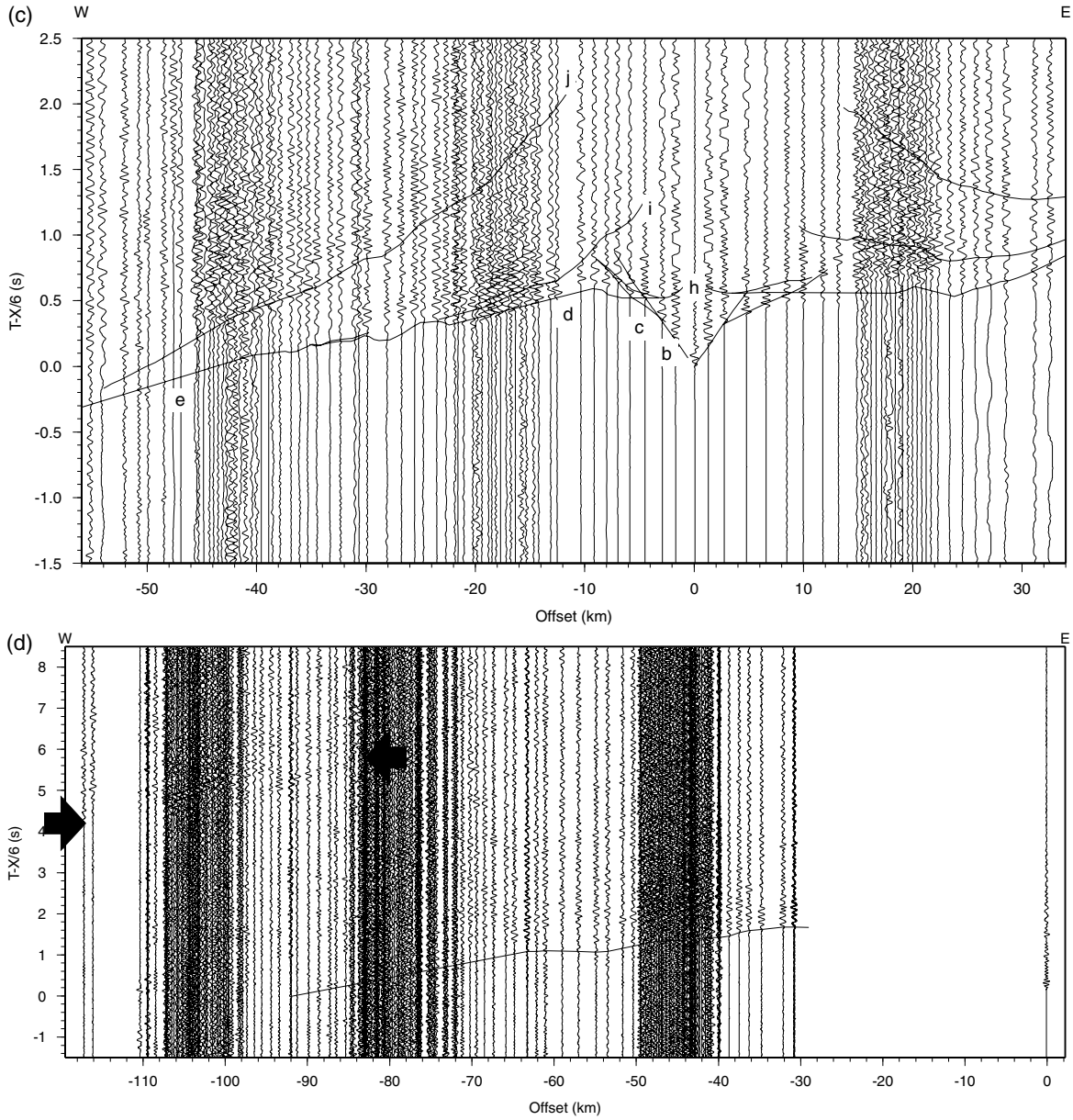

Figure 3. (*Continued.*)

velocities dip eastwards with the 6 km s^{-1} contour at ∼2 km depth beneath KAM and ∼4 km depth beneath KEL_PYL.

Seismic ray tracing

A more structurally oriented layer-based model (Fig. 5) was then derived via traveltime modelling of the refracted and reflected phases. This was conducted using a combination of forward modelling and inversion with the RAYINVR code of Zelt & Smith (1992). In order to minimize the errors associated with the assumption of a 2-D profile, especially in the near surface, it was decided to model the shallow (<5 km) structure as three distinct profiles: KAM–NIK, NIK–MAT and MAT–KEL_PYL. These were then merged and used as a starting model for modelling the deeper structure as one profile. Initial models were obtained through trial and error forward modelling to fit the picked traveltimes using a top-down layer stripping approach. These models were then refined via damped least squares inversion to minimize the traveltime residuals. The resultant traveltime velocity model was subsequently refined, mainly regarding the vertical velocity gradients, based on qualitative comparison of the record sections with synthetic seismograms calculated using the TRAMP code of Zelt & Forsyth (1994).

The seismic ray trace model

The final velocity model obtained with the seismic ray tracing method is shown in Fig. 5. An intermittent upper layer of velocity 2.5–3.0 km s^{-1} is modelled with a variable thickness from AYI to POL and again to the east of LYM. A second layer of velocity 3.3–3.7 km s^{-1} extends from APL eastwards with thicknesses varying between 0.2 and 1 km. Beneath these layers is a 1 km thick layer of velocity 4.6–5.0 km s^{-1} thickening to the eastern end of the profile. This layer outcrops between KAM and APL, where its velocity is slightly lower than elsewhere, and deepens to the east. The interface

Table 1. Average picking errors assigned to each traveltime phase.

Descriptor	Assigned error (s)
Refraction in near surface layer (sediments/volcanics)	±0.05
Refraction in layer 2 (volcanics)	±0.05
Refraction in layer 3 (SDC)	±0.05
Reflection from base of layer 3	±0.07
Refraction in layer 4 (Gabbros)	±0.05
Reflection from base of layer 4	±0.10
Refraction in layer 5 (Ultramafics/Plutonics)	±0.07
Moho reflection PmP	±0.15
Mantle diving wave Pn	±0.08
Mantle reflector	±0.20

at the base of this layer is irregular with major steps of up to 500 m which correlate with similar steps in the top interface of the layer. It is underlain by a layer with velocities between 6.05 and 6.67 km s^{-1}. The highest velocities are in the central section of this layer with lower velocities at the eastern and western ends of the profile. Between KAM and KEL_PYL this layer thickens eastwards from 3.6 to 6.5 km. The base of the layer also deepens eastwards from ∼2.5 km beneath KAM to 11 km beneath KEL_PYL. Beneath the extreme shotpoints at AKA and PAR this layer is apparently much deeper, although exact depths are difficult to model due to the lack of traveltime information. A 6 km thick layer of velocity 6.9–7.1 km s^{-1} is modelled beneath this layer. The base of this layer is shallowest beneath APL, beneath which it is underlain by material of 8 km s^{-1}, but sampled only by an unreversed diving wave from AKA.

Resolution analysis

Traveltime fits were assessed for both inversion methods by monitoring the number of rays traced, the rms traveltime residual and the normalized form of the misfit parameter, χ^2(Table 2) (Zelt & Forsyth 1994; Zelt 1999). The rms traveltime residual generally decreases with each iteration until a minimum is reached. The misfit parameter χ^2 also in general reduces with each iteration, with unity indicating a good solution within the picking uncertainties. Values much less than 1 indicate that the data have been overmodelled, that is, they have been fit closer than is justified by the uncertainties and the model may contain structure that is not required. A χ^2 value much greater than 1 generally indicates that the data have sampled small-scale heterogeneities that cannot be resolved (e.g. the cell spacing of the tomography model may be larger than the structure) or are affected by 3-D structure.

The ray coverage of the model is also important in assessing the suitability of the final model. Ray coverage is shown in terms of the ray density for the tomographic model (Fig. 6a), that is, the number of rays sampling each node or cell of the model. For the RAYINVR models it is given in terms of ray diagrams (Fig. 7) showing the two-point ray paths connecting the shot and receiver whose associated times are the earliest for a particular receiver or phase (Zelt 1999). Fig. 6(b) also shows the traveltime misfit for the final tomographic model.

Errors associated with the interface depths and velocites have been assessed through model perturbation and are estimated as 0.2 km s^{-1} for the velocities of the upper three layers and 0.3 km s^{-1} for the lower three layers. The interface depth errors are estimated as 0.15, 0.15, 0.25, 0.5 and 1 km for the five layer boundaries.

Gravity data processing and modelling

The gravity data reduction to calculate the Bouguer anomaly followed the standard method outlined below:

(1) Conversion to the observed gravity value with reference to the Malounda base station value of 979 835.95 mgal.
(2) Calculation of the theoretical sea level gravity using the 1967 International Gravity Formula (IAG 1971).
(3) Calculation of the free air anomaly (FAA).
(4) Calculation of the simple Bouguer anomaly (SBA) using a replacement density of 2.67 g cm^{-3} (Shelton 1993).
(5) Calculation of the corrected Bouguer anomaly (CBA) through the application of terrain corrections to a standard outer zone radius of 167 km and accounting for the curvature of the Earth (Swain & Khan 1977).

The Bouguer anomaly profile (Fig. 8) shows a positive anomaly associated with the ophiolite, decreasing eastwards. The troughs either side of this are likely associated with the Polis Graben to the west and the circum-Troodos sedimentary succession to the east. The Mt Olympus negative anomaly is not observed as the survey lies to the north of the anomaly centre.

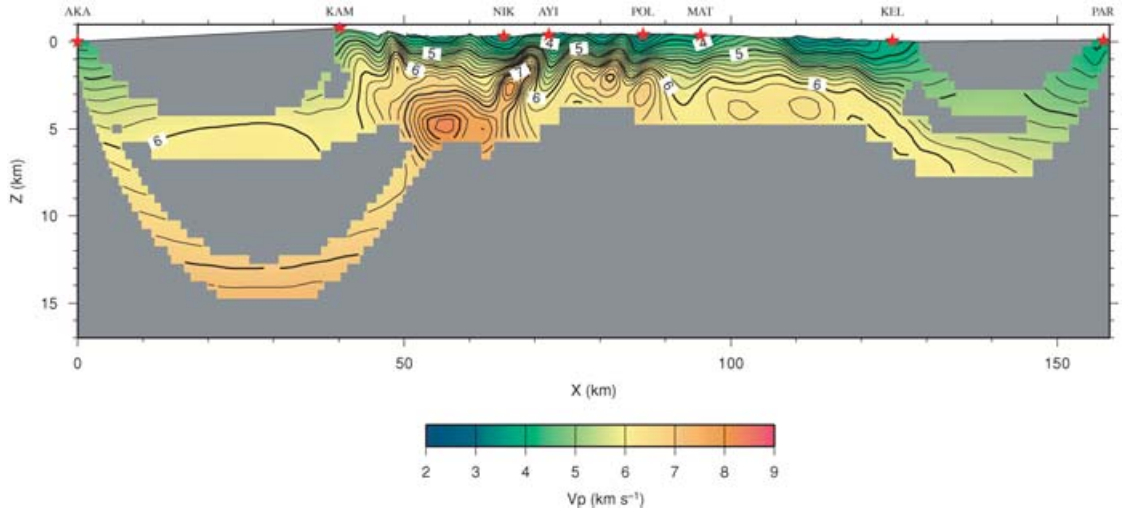

Figure 4. 2-D tomographic velocity model of the Troodos ophiolite from modelling of first arrival times using the FAST code of Zelt & Barton (1998). Areas with no ray coverage have been masked. Velocity contours are shown every 0.2 km s^{-1}.

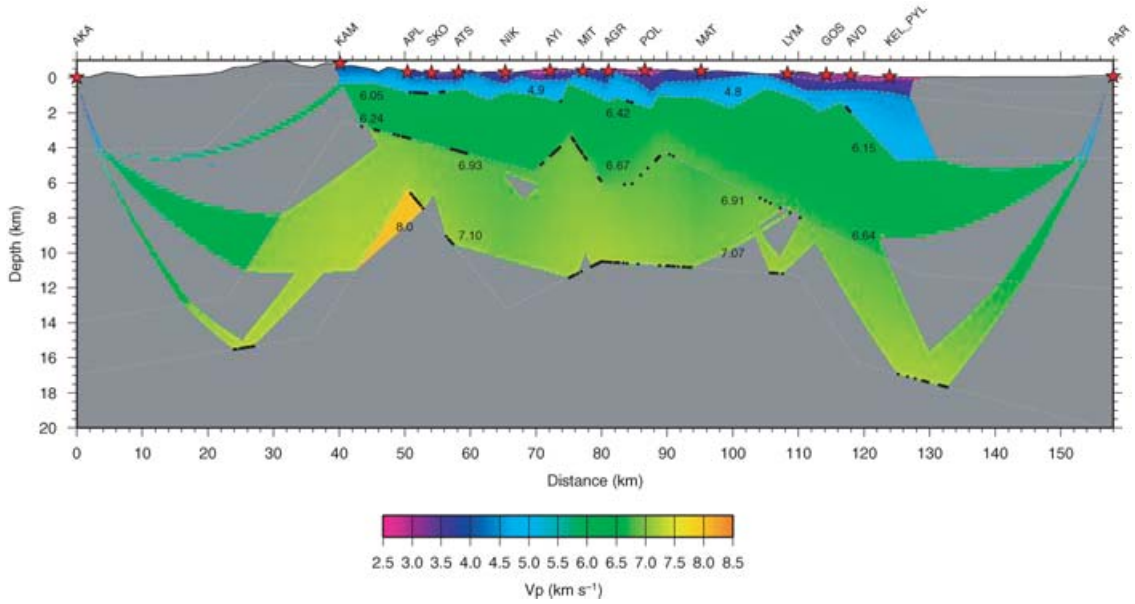

Figure 5. 2-D velocity model of the Troodos ophiolite obtained from ray tracing using RAYINR (Zelt & Smith 1992). Modelled interfaces are indicated by dashed grey lines with bounce points of modelled reflected phases indicated by the black points. Areas with no ray coverage have been masked out.

Table 2. Summary of modelling results for the tomographic and layer based modelling. N is the number of picks (percentage indicates percentage of data points used), $T_{\rm rms}$ and χ^2 after Zelt & Forsyth (1994). Models D1, D2 and D3 are for the shallow (<5 km) structure.

Model	N	$T_{\rm rms}$	χ^2
FAST starting	1067	0.516	41.42
FAST final	1067	0.125	2.38
D1: KAM–NIK	283 (90 per cent)	0.033	1.01
D2: NIK–MAT	428 (87 per cent)	0.041	1.01
D3: MAT–KEL	283 (83 per cent)	0.058	1.28
Single profile	1388 (83 per cent)	0.063	1.89

Gravity modelling was conducted using the 2.5-D gravity and magnetic modelling software GRAVMAG (Pedley *et al.* 1993). A 2-D density model was created using the interfaces defined by the seismic model and assigning densities to these layers. The maximum depth of the model was 30 km, and the model was linearly extended to ±1000 km beyond the limits of the seismic profile to reduce end effects. Initial density values were assigned using a combination of (a) the conversion of modelled seismic velocities to density values using empirical relationships (e.g. Bartetzko *et al.* 2005; Christensen & Salisbury 1975), (b) measured density values from hand specimens and boreholes cores (Smith & Vine 1987, 1989, 1991; Salisbury *et al.* 1989), (c) previous density modelling (Shelton 1993) and (d) modern oceanic analogues (e.g. Carlson & Herrick 1990). The anomaly calculated from this initial starting model had a reasonably close fit to the CBA data, lending confidence to the seismic model. The major disparities required the long-wavelength positive anomaly over the Troodos complex to be extended towards both ends of the profile, and the presence of a short wavelength anomaly 'trough' in the region around Mathiatis (MAT) (Figs 1 and 2).

The initial model was refined to provide a final density model giving a theoretical anomaly that closely matches the observed (Fig. 8). The perturbation of the layer interface depths and densities was controlled by the resolution of the seismic model with larger perturbations allowed where resolution was poor. Final velocity and density values for each layer are shown in Table 3.

The final density model (Fig. 8c) shows a similar structure to the seismic model involving eastward dipping layers, the deeper levels progressively outcropping to the west. The major offsets in the layer boundaries beneath ATS, MIT and AGR have become more distinctive and an offset in the upper layers beneath GOS has also become apparent. The sediments of the Polis graben and within the circum Troodos sedimentary succession are modelled as being ∼4 km thick but this is very poorly constrained. The principal difference between the gravity and seismic models is in the lateral extent of the ophiolite sequence and a thickening of the surface layer (density 2.31 g cm^{-3}) beneath MAT. This latter is consistent with the higher resolution seismic refraction results of Cooper (1993) which demonstrated a north-eastward thickening of the sediment and extrusive layer including the basal group, from 750 to 1.5 km depth over a 12 × 12 km^2 area in the vicinity of Mathiatis. The difference between the seismic and gravity models in the vicinity of MAT may be explained by the presence of 3-D effects, the seismic line changing orientation in this region from NW–SE to E–W (Fig. 2). In addition surface geology indicates that there is a rotation in the principal direction of the geological structure here (Constantinou 1995) such that the seismic line runs parallel to structure as opposed to transecting it. The resolution of the shallow region of the seismic model is poor at the edges of the three deployments where the station spacing is less dense and there is low ray coverage (Fig. 7) so the lateral 'extension' is not inconsistent with the seismic data.

INTERPRETATION

Based on drillhole information and surface geology a simple geological interpretation (Fig. 9) of the geophysical models has been made. Results from the IANGASS survey are tabulated alongside velocity values from relevant borehole and seismic results in Table 4. Discussion of the results in relation to those obtained from oceanic crust is considered later.

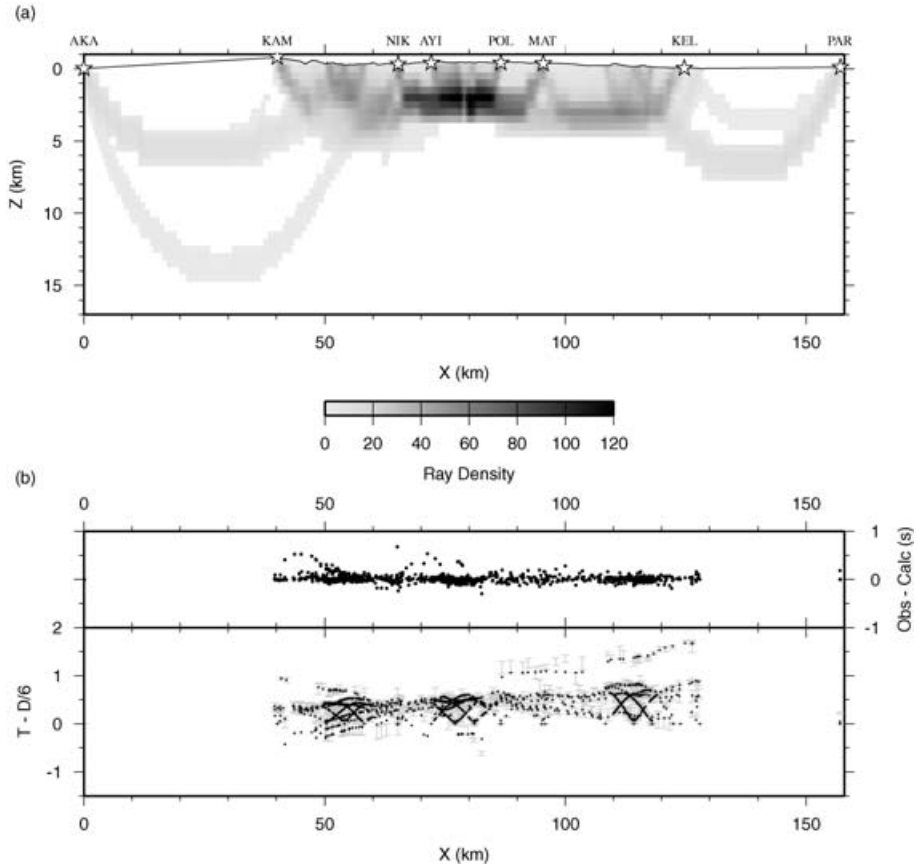

Figure 6. Resolution of the tomographic velocity model. (a) Ray density diagram (b) traveltime misfit (upper) and modelled and observed first arrival traveltimes (lower). Note the *ca*. 0.5 s delay in first arrivals from shotpoint PAR due to ray paths through the circum Troodos sedimentary succession. A similar but smaller delay can also be observed on the arrivals from shotpoint AKA.

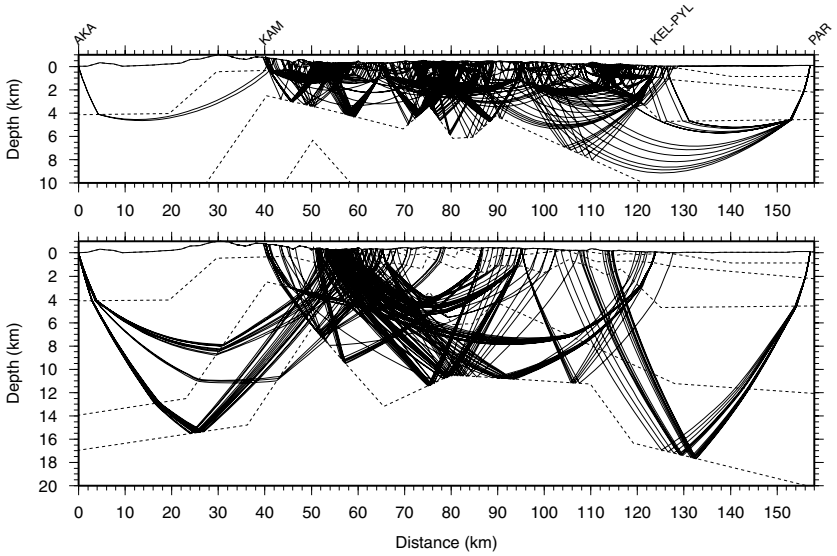

Figure 7. Two-point ray path diagrams for the sediments, volcanic, SDC and gabbroic layers (upper) and ultramafic/plutonic layer (lower).

Sediments and extrusives

The velocity and density of the upper two layers correspond well with samples from CY-1, 1a and CY-2, 2a drill cores (Fig. 10), the downhole logging results and the results from delay time analysis of short refraction profiles by Lort & Matthews (1972). They are interpreted as resulting from a combination of sediments and the upper pillow lava sequence (velocity 2.5–3.0 km s^{-1}) underlain by the lower pillow lava sequence consisting of pillows and massive flows (velocity 3.3–3.7 km s^{-1}). The modelled layers also correlate well with surface outcrop. The resolution of the models does not

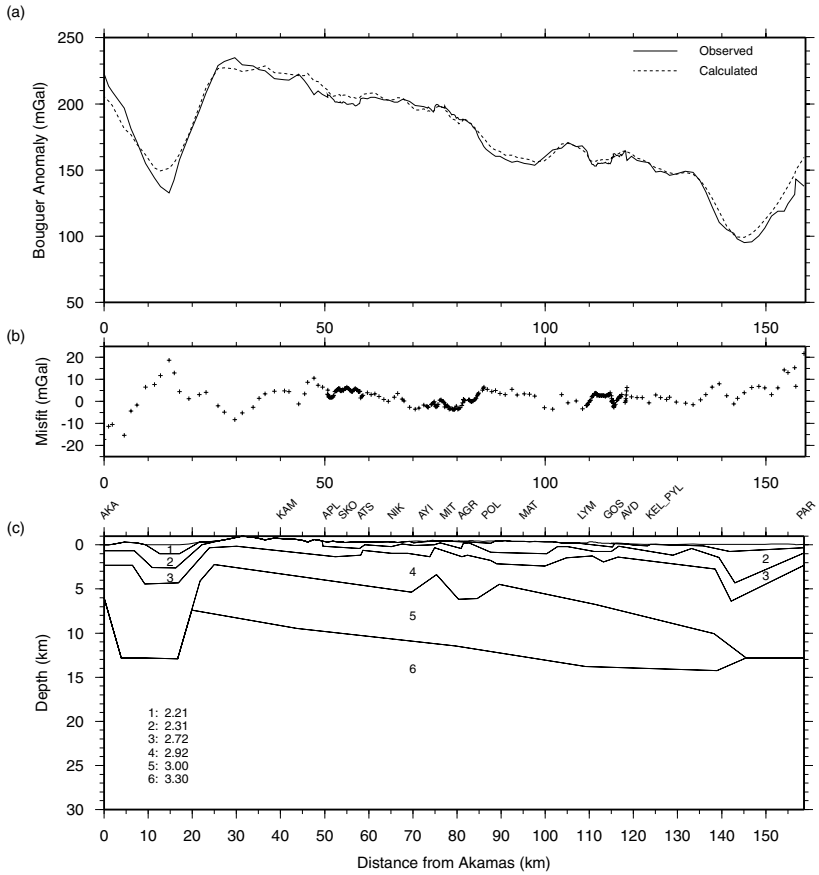

Figure 8. (a) Observed and final calculated Bouguer gravity anomaly along the IANGASS 1995 profile (b) Bouguer anomaly residual (observed–calculated) (c) Final density model of the Troodos ophiolite (shotpoint identifiers as for Fig. 2).

Table 3. Layer velocity and density values for the final seismic and gravity models.

Layer	Velocity (km s^{-1})	Density (g cm^{-3})
1: Sediments & UPL	2.5–3.0	2.21
2: LPL	3.3–3.7	2.31
3: SDC	4.6–5.0	2.72
4: Gabbro	6.05–6.67	2.92
5: Ultramafic	6.91–7.10	3.00

UPL, upper pillow lavas; LPL, lower pillow lavas.

make it possible to resolve the sediments from the upper pillow lava sequence.

Sheeted dyke complex

The underlying layer of velocity 4.6–5.0 km s^{-1}, density 2.7 g cm^{-3}, is interpreted as the sheeted dyke complex. The outcropping of this layer to the west of APL also correlates well with surface geology and it is probable that the lower than average velocities in this region are a result of more extensive weathering and lower overburden pressure resulting in a higher crack density. The velocity of this layer correlates well with the results from short refraction profiles (Lort & Matthews 1972), with the exception of one very low value from the short profile survey. The velocity and density of this layer also correlate well with values of 4.63–4.82 km s^{-1} for the sheeted dykes obtained from CY-1, 1a and CY-2, 2a (Smith & Vine 1987, 1991). CY-4 sampled the lower part of the sheeted dyke complex (Smith & Vine 1989) and compressional wave velocities increased from approximately 5.4 km s^{-1} at the top of the drill hole to 6.8 km s^{-1} at the base of the sheeted dykes (Salisbury *et al.* 1989) with a mean of 6.50 km s^{-1} (Smith & Vine 1989). The sheeted dykes and the underlying gabbro in CY-4 are less pervasively metamorphosed than dykes exposed in other areas of the ophiolite (e.g. Bickle *et al.* 1998) and it is possible that the lower extent of hydrothermal alteration has led to the higher average velocity for this unit in CY-4 than throughout the rest of the ophiolite. This is further discussed below.

Between SKO and MIT the sheeted dyke layer averages ∼800 m thickness with an average velocity of 5.0 km s^{-1} making it comparable to the second layer of Khan *et al.* (1972). The boundary between the lavas and sheeted dykes is defined primarily by seismic diving waves and does not preclude the presence of the gradational basal layer above the sheeted dyke complex.

Several large (up to ∼500 m) offsets modelled in these upper layers, some extending into the layer beneath the sheeted dykes, are interpreted as faults. These are all apparently downthrown to the west, and are interpreted as syn-volcanic growth faults based on evidence for a relatively smooth lava - sediment interface across the ophiolite, and the apparent thickening of the lava sequence towards them (Fig. 9). These faults are approximately evenly spaced with separations ranging from 5.6 to 8.4 km perhaps suggesting a systematic control on when a new major fault nucleates. Detailed geological mapping studies have identified both the eastern most and western most faults. Hurst *et al.* (1994) mapped a major, down-to-the-west fault running almost N–S through Kakopetria and just east

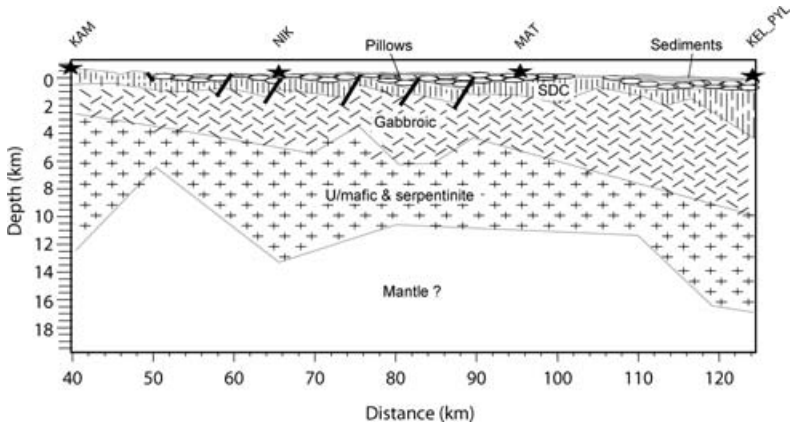

Figure 9. Simple geological interpretation of the Troodos ophiolite based on the seismic and gravity models shown in Figs 4, 5 and 8.

Table 4. *P*-wave velocities compared with sample core and borehole seismic results from Troodos and oceanic crust.

Unit	This study	CY-1,1a[a]	CY-2,2a[b]	CY-4[c]	Logged boreholes[d]	Short refraction lines[e]
Sediments	2.5–3.0					–
Lavas	2.5–3.7	3.47–3.55	3.49		3.2–3.5	2.8-3.7
Basal Unit					5.0	2.9–4.8
SDC	4.6–5.0	4.82 (top)	4.2–5.17	6.50	5.0–6.4	3.0–5.1
Gabbros	6.05–6.67			6.93	6.7–6.9	5.5
Ultramafics	6.91–7.10			7.26	7.0-7.4	2.5-4.2

Sample cores from Troodos boreholes: [a]CY-1, 1a (Smith & Vine 1991); [b]CY-2, 2a (Smith & Vine 1987); [c]CY-4 (Smith & Vine 1989).
Downhole logging of Troodos boreholes: [d](Salisbury *et al.* 1989).
Short refraction profiles: [e](Lort & Matthews 1972).

of SKO. This corresponds closely in both location and interpreted throw with the the fault identified in the seismic data near ATS. Likewise, Taylor (1983) mapped a major syn-volcanic growth fault near Politiko (POL) with a throw of 600–800 m dropping down-to-the-west. The basin formed here was filled by volcanics leading to a smooth lava-sediment interface (fig. 3.21 in Taylor 1983). While we have not identified a direct correlation between the other modelled faults and those on the ground, the presence for example of 'a 100-m-wide breccia zone that projects northwards—toward the large Agrokipia and Kokkinoyia massive sulfide mines' (Varga & Moores 1985) is consistent with the location of the fault we interpret as lying beneath the AGR shotpoint.

Gabbroic layer

The 3–6 km thick layer beneath the sheeted dykes, with velocity 6–6.7 km s^{-1} and density 2.9 g cm^{-3}, is interpreted as comprising gabbroic rocks, probably including ultramafic plutonics. The relatively low velocity of this layer beneath KAM may be the result of increased fracturing in this area occurring during the recent uplift of Mt Olympus. Between SKO and MIT the velocity and thickness of this layer is comparable to that determined for layer 3 by Khan *et al.* (1972). The velocity of this layer is significantly larger than that derived by Lort & Matthews (1972) for gabbroic rocks (5.5 km s^{-1}); however, they suggest that their results are 'surprisingly low' and may result from both increased porosity and the rocks not being water saturated owing to their being at the surface.

Ultramafic or serpentinite layer

The base of the gabbroic rocks at 4–8 km depth from west to east is underlain by a very thick (6 km) layer of $V_P > 7$ km s^{-1} with a density of 3.0 g cm^{-3}. This basal layer may be partially serpentinized peridotite or ultramafic cumulates or fresh peridotite including some mafic intrusions. If it is serpentinized peridotite then both the velocity and density would be consistent with *ca*. 40 per cent serpentinization, similar to the extent of serpentinization of the mantle section of the ophiolite (Wilson 1959; George 1978); this does not include the serpentinite diapir which is genetically unrelated to the ophiolite (Robertson 1998; Batanova & Sobolev 2000).

Base of the model

The seismic model is almost completely unconstrained beyond either end of the ophiolite complex. However, we have modelled reflections at a depth of ∼16 km to the west of the ophiolite, and ∼18 km beneath the eastern sediments. Beneath the western end of the ophiolite itself, an unreversed velocity of 8.0 km s^{-1} might suggest that 'normal' mantle underlies the postulated serpentinized peridotite or ultramafic cumulate layer, but again, this is very poorly constrained. If the material beneath the deepest reflections is 'normal' mantle, then this is significantly different from the model of Makris *et al.* (1983) who proposed continental crust above a Moho at 35 km depth beneath the Polis graben, and that of Ergün *et al.* (2005) who similarly proposed continental crust, but here above a Moho at ∼20 km depth beneath the exposed Troodos ophiolite. This discrepancy is discussed below.

A reflection from the present-day slab?

Assuming typical mantle velocities beneath our model, simple 1-D modelling of the deep reflection visible on the seismic section from PAR (Fig. 3d) indicates that this originates from a reflector

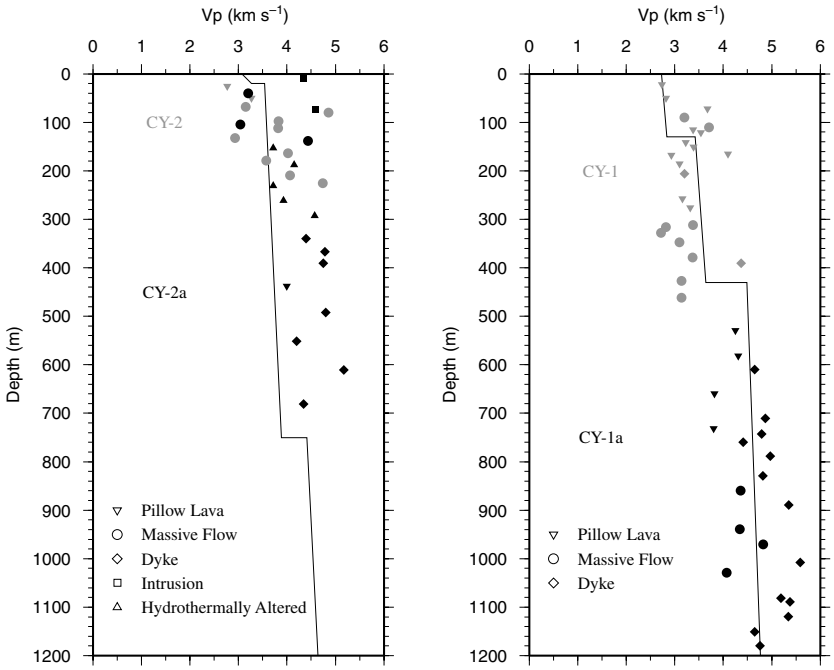

Figure 10. Comparison of the modelled velocity with core samples at well CY-1, 1a and CY-2, 2a.

at ∼55 km depth. At this depth the reflection could originate from the northward dipping slab arising from the subduction of the Sinai microplate beneath Cyprus (e.g. Mascle *et al.* 2000). The existence of this slab is also suggested by regional gravity modelling (Ergün *et al.* 2005). The exact depth to this reflector is uncertain, being derived from an unreversed seismic traveltime section.

DISCUSSION

(1) *Comparison between the Troodos seismic model and seismic models of oceanic crust*

The Troodos ophiolite has played a pivotal role in the development of concepts concerning the processes of sea-floor spreading (e.g. Robertson & Xenophontos 1993). However, comparison between our model parameter values (velocities and densities), and those of modern oceanic crust, suggests differences between the Troodos ophiolite and oceanic crust that need to be explained. That said, it should be emphasized that the structural interpretation concerning the presence of syn-volcanic growth faults observed to offset the sheeted dyke gabbro boundary and the lava—SDC boundary, depends primarily on the distribution of velocity values themselves, rather than their interpretation in terms of lithologies.

It is now generally accepted that beneath the oceanic sediments (oceanic seismic layer 1) there is not a simple one-to-one correlation between the three part ophiolite lithological layering (basalts, sheeted dykes, gabbros) and the equivalent oceanic two-layer seismic velocity structure of layer 2 (being on average 2 km thick with velocities increasing from 3 to 4 km s^{-1} at the top to >6.5 km s^{-1} at the base) above layer 3 (with velocities commonly in the range 6.7–7.0 km s^{-1}) (Carlson & Miller 2004).

It is also known that seismic velocities are scale dependent, being affected by the variable distribution of porosity and alteration at core sample, borehole and crustal seismic survey scale. Not only this, but seismic velocity in the oceanic crust, which is known to be anisotropic (e.g. White & Whitmarsh 1984; Swift & Stephen 1989), has also been shown to contain horizontal gradients (e.g. of >2 s^{-1} in the upper crust over a scale of 1–2 km) comparable to its vertical gradients (e.g. Stephen 1988).

The methodology used here (interpreting the arrival times of refracted and reflected seismic rays derived from a relatively poorly sampled profile of irregularly distributed shots and recorders over severe topography and highly weathered surface material) results in a simple layered model with a limited range of velocities derived for each layer. Accepting that the values derived from borehole and laboratory sample may be significantly different as outlined above, there is also the likelihood of values derived from crustal scale seismic surveys also being different. Carlson (1998) has described the various experimental procedures used to derive crustal scale velocity models of the oceanic crust. In general the redundancy of data, the regularity of source and receiver spacings, the uniformity of sources used, as well as the uniformity of near surface conditions enable the use of processing and interpretation methods which provide crustal models involving continuously increasing velocity functions with depth. These better reflect the continuous variation, for example from extrusives to sheeted dykes which is known to exist, than the apparent distinct uniform layering for each of these units, as derived in our model.

Because of these difficulties, our model which defines the derived seismic velocities in terms of Troodos ophiolite lithologies by comparison with surface outcrop and borehole log and sample correlation, cannot be easily related directly to oceanic crustal velocities, but a number of points can be made.

First, given the limitations identified above, there is good correlation between our modelled velocities for the sediments and lavas and those derived for oceanic crust (Table 5).

Secondly, the correlation with the velocity values derived from sheeted dykes in holes CY-1, 1a (Smith & Vine 1991) and 2 (Smith & Vine 1987) which are closest to our profile, and our values obtained over outcropping sheeted dykes at the western end of the profile, suggest these correlations are robust. However, comparison of our results with those of normal oceanic crust (e.g. Carlson & Herrick

Table 5. *P*-wave velocity values derived for oceanic seismic layers 1–3 from both typical oceanic crust (Carlson & Herrick 1990) and Hole 504B .

Oceanic layer	Typical ocean	ODP 504 B		
		Sonic data	Laboratory sample measurements	Wide-angle seismic[e]
1	2.2		1.55–4.6[c]	1.6
2A	2.5–3.2	4.0-5.0[a] 3.35-6.35[b]		5.0
2B	5.25	4.8-6.0[a]		6.5
2C	6.10	6.0[a]	6.2–6.7[d]	6.7
3	6.8			7.1

[a]Salisbury *et al*. 1985, [b]Moos *et al.* 1986, [c]Wilkins & Langseth 1983, [d]Christensen *et al.* 1989, [e]Collins *et al.* 1989.

1990) and those sampled in Hole 504B (Wilkins & Langseth 1983; Salisbury *et al.* 1985; Moos *et al.* 1986; Christensen *et al.* 1989; Collins *et al.* 1989) (Table 5) would suggest that the velocities in the Troodos sheeted dyke complex are significantly less than those in oceanic crust. However the average thicknesses are equivalent. A number of factors may explain this discrepancy:

(i) One reason for the low value of the velocity in the sheeted dykes derived from our study is likely to be the significant tectonic disturbance suffered by the dykes on Troodos, both as a result of initial sea-floor spreading processes in this supra-subduction zone environment, and also the updoming which resulted in the emergence of the plutonic sequence at the heart of Troodos within the last 2 Myr. This has resulted in the complex being dissected by fractures and faults at a wide variety of scales, which will reduce the seismic velocity in relation to that of pristine, undeformed oceanic crust.

(ii) As discussed in relation to the high velocity values obtained for the sheeted dykes in CY-4, the dykes of the Troodos ophiolite are substantially more hydrothermally altered than those of the modern ocean floor (e.g. at Hole 504B) which may have reduced their velocity. The formation of hydrous secondary minerals, and increases in porosity related to metamorphic reactions, can lower the compressional wave velocity (Christensen *et al.* 1989).

(iii) Swift *et al.* (1998) examined seismic anisotropy within Hole 504B comparing (vertical) velocities derived from Vertical Seismic Profiles (VSP) and (horizontal) velocities derived from Offset Seismic Profiles (OSP). They conclude that the vertical velocities may be up to 10 per cent higher than the horizontal velocities, which is consistent with our velocities (derived from subhorizontal refracted/diving waves) for the sheeted dykes being less than those identified in Hole 504B using VSP.

(iv) The other factor that we should consider is whether the sheeted dyke/gabbro boundary that we have identified can be equated to the Layer 2/3 boundary at all. There have been numerous studies commenting on this correlation. A number of these have resulted from study of the compressional wave structure in Hole 504B (Wilkins & Langseth 1983; Salisbury *et al.* 1985; Moos *et al.* 1986; Christensen *et al.* 1989; Collins *et al.* 1989; Detrick *et al.* 1994; Swift *et al.* 1998; Sun & Goldberg 2000), and more recently in Hole 1256D (Wilson *et al.* 2006). The principal result is that factors including porosity and alteration are more important than rock type (or grain size) in controlling the boundary between layers 2 and 3, necessitating caution in accepting exact correlation between lithology and the deeper layers of our model. Detrick *et al.* (1994) examining seismic refraction data suggest that the seismic Layer 2/3 boundary lies within the sheeted dyke sequence. Swift *et al.* (1998) using VSP in Hole 504B produced results implying that seismic Layer 2 is composed of the extrusive layer and the transition layer in which pillows, flows and intrusive dykes intermix. The upper portion of Layer 3 (velocity $\sim$6.1 km s^{-1}) is composed of the lower section of sheeted dykes. Wilson *et al.* (2006) from downhole velocity measurements in Hole 1256D identify the layer 2/3 boundary below the depth at which gabbro was first encountered. In the light of these observations, while accepting that the ophiolite velocities are low for the reasons outlined above, we suggest it is possible that the SDC/gabbro boundary may lie within the 6.05–6.67 km s^{-1} layer, deeper than the modelled reflector we have interpreted as this boundary. However, given the errors associated with our interface depth estimates, documented in 'Resolution Analysis' in the Data Modelling section above, it is unlikely we could resolve the difference in depth to the oceanic lithological and seismic layer boundaries.

(2) *Crustal thickness and implications for generation of Troodos oceanic crust*

The nature of the basal layer ($V_P > 7$ km s^{-1}; 3 g cm^{-3}) is critical to the interpretation of the thickness of the original supra-subduction zone oceanic crust and hence the amount of melt generated. If this layer is comprised largely of serpentinized mantle then the Troodos crust is only $\sim$5 km thick—slightly thinner than average crust formed at fast spreading ridges but probably similar to that at some slower spreading ridges. This would be somewhat surprising because the large amounts of water that must have been added to the Troodos mantle (Muenow *et al.* 1990) should have led to increased melt production over that at mid-ocean ridges and would either require a depleted mantle source and/or inefficient melt generation or extraction beneath the ophiolite (e.g. Martinez & Taylor 2002; Coogan *et al.* 2002). Alternatively, if the basal layer is composed largely of ultramafic cumulates, this would indicate that substantially more melt was generated beneath the Troodos ophiolite than at a normal mid-ocean ridge.

Mass balance calculations, based on the composition of the lavas, dykes, mafic cumulates and ultramafic cumulates recovered by drilling in the Troodos ophiolite allow us to reconstruct the possible bulk crustal compositions in either end-member scenario. Using the lava and dyke compositions from CY-1,1a and the mafic and ultramafic cumulate compositions from CY-4 (Banks 2004) we can compare the composition of the bulk crust for the thick and thin crust scenarios. The thick crust has a bulk Mg# of 79.4, MgO of 14.8, CaO of 13.3 and Al_2O_3 of 9.6. The thin crust has an Mg# of 72.9, MgO of 11.6, CaO of 11.5 and an Al_2O_3content of 12.8. Although there are uncertainties in the average composition of each layer, which degrade the accuracy of these estimates, the relative differences are well constrained. That said, the thick crust model has an unrealistic composition with too high a Mg#, too low an Al content, and much too high a Ca/Al ratio. This is true even given the uncertainties in the composition of the source, pressure and temperature of melting, and uncertainty in the bulk crustal composition. We conclude that without *S* wave data to pin down the degree of serpentinization, it is not possible to unambiguously distinguish the nature of the basal

layer. However, we favour a serpentinized mantle, or mixed mantle and mafic cumulates, origin for this layer

(3) *Nature of the material underlying the basal layer* ($V_P > 7.0$ *km* s^{-1})

It is not possible from our model to define the nature of the material underlying the basal layer of velocity >7.0 km s^{-1}. However, we speculate that it is mantle peridotite. This is consistent with the observation of an unreversed velocity of 8.0 km s^{-1} identified at the western end of the IANGASS profile beneath shotpoint APL. While this is obviously inadequate proof, our model and interpretation is consistent with that of Shelton (1993). In addition, petrological constraints support such a hypothesis. The Mount Olympus serpentinite is compositionally distinct from mantle peridotite underlying the ophiolitic crust (Batanova & Sobolev 2000). The latter had a large amount of basaltic melt extracted from it during the formation of the Troodos ophiolite and is only ∼40 per cent serpentinized. The Mount Olympus serpentinite is not simply related to the ophiolite, rather it is believed to result from fluids from the subducting slab serpentinizing the overlying mantle (Robertson 1998). This serpentinized peridotite has risen diapirically to the surface within the last few Myrs. Two arguments suggest that this serpentinite diapir has not penetrated through continental crust on its way to the surface. First, the diapiric serpentinite body would not have had sufficient density contrast to rise through continental crust. Secondly, it would be expected to entrain continental crustal material for which there is no evidence.

The discrepancy between this hypothesis and the results of Makris *et al.* (1983) needs to be explained. They predict 35 km thick continental crust beneath western Cyprus (including the Polis graben). Beneath the Polis graben our seismic model is extremely poorly constrained and a significant underestimate of the crustal thickness beneath this part of our model is possible. Given that this region is also at the end of the seismic profile of Makris *et al.* (1983) it is also not unreasonable to expect that their model may also be poorly constrained in this region.

The Makris *et al.* (1983) model was used to help build the intial model of Ergün *et al.* (2005) who predict a ∼20 km thick continental crust beneath the western part of the exposed ophiolite. This crustal thickness of ∼20 km derived from gravity modelling occurs over Troodos itself, assumes a mantle density of 3.38 g cm^{-3} (as used by Makris *et al.* 1983). However, serpentinized mantle has a lower density and, based on the recent diapiric upwelling of serpentinized peridotite to form Mt Olympus, it seems likely that much of the mantle beneath Cyprus may be partially serpentinized by fluids from the subducting slab (see e.g. Hyndman & Peacock 2003). Based on this we have used a lower density for the mantle whereas the mantle beneath Makris *et al*'s (1983) profile is less serpentinized and therefore of higher density, consistent with an equivalent Bouguer Anomaly being modelled with their very much thicker, but lower density, continental crust.

(4) *Implications for models of crustal tectonism in the Troodos ophiolite*

Two types of model for tectonic extension in the Troodos ophiolite have been proposed which are as follows.

(a) The earlier models, based on the orientations of dykes within the sheeted dyke complex, suggested three graben structures although the origin of the grabens has been controversial (Varga & Moores 1985; Allerton & Vine 1987). Varga & Moores (1985) proposed that there are three fossil ridge-axis grabens preserved within the Troodos ophiolite that record the eastward stepping of the spreading axis. The western-most, Solea graben, is the most extensively studied. The geophysical models derived here (Figs 5, 8 and 9), provide evidence for a large fault offsetting the lava/dyke boundary beneath ATS on the eastern side of the proposed graben. However, while a fault may be interpreted beneath APL on the western side of the graben, which correlates with the location of the down-to-the-east Troodos Forest fault mapped by Hurst *et al.* (1994), the models provide less evidence that this is a major graben-bounding fault. The central, or Mitsero graben between AYI and POL, should be well constrained by the seismic line but there is no evidence for this feature in the data. The eastern, Larnaca graben between LYM and AVD, should also be relatively well constrained by the data, but once again, there is no evidence for this in the seismic model. Cooper (1993) suggests that the northern margin of the ophiolite in the vicinity of Mathiatis is downfaulted beneath the overlying sediments, occurring as a result of N–S directed emplacement. While the strike of our seismic profile subparallels the strike of the proposed faults in this region, their lack of expression in our seismic data would suggest that they are not the cause of the large faults offsetting the extrusive—SDC and SDC—gabbroic layer horizons in our final model (Fig. 9).

(b) Agar & Klitgord (1995) proposed an alternative to the graben model for tectonic extension within the Troodos ophiolite. They suggested that deformation is decoupled between the sheeted dyke complex and the plutonic complex leading to different kinematic histories for these units. However, they also suggest that major faults, dipping towards the ridge axis, cut this boundary as observed in the seismic and gravity models. Because the resolution of the geophysical models is insufficient to identify a thin decoupling zone between the sheeted dykes and the plutonic complex, the seismic and gravity data cannot test this model directly. However, Agar & Klitgord (1995) propose a spreading centre to the east of the ophiolite based on the structures they observed. This contrasts with the down-to-the-west faults interpreted from our results that suggest a spreading centre to the west of the ophiolite. Such a model would be consistent with the dyke chilling statistics of Kidd & Cann (1974) and Baragar *et al.* (1990) and microfossil ages (Osozawa & Okamura 1993).

In contrast to these existing models the seismic data is most readily interpreted by a model in which major normal faults, downthrown towards the ridge axis, formed at regular intervals. These faults must have formed close enough to the ridge axis that either long lava flows, or off-axis volcanism, could fill the developing half-graben. These faults remained active for an extended period, accumulating throws of up to 500 m, before deformation jumped to a new fault closer to the ridge axis.

CONCLUSIONS

Velocity and density modelling of the Troodos ophiolite complex has been completed using the seismic and gravity data sets acquired during the IANGASS 1995 geophysical project. The results of this modelling are as follows.

(i) A five layer structure is modelled. The velocities and densities of the upper layers are consistent with measured borehole properties of the sediments, pillow lavas, sheeted dykes and a gabbroic layer. Although the modelled velocities are in general lower than the equivalent velocities from oceanic crust there are a number of factors that may account for this. While we are unable unambiguously to define the composition of the thick basal layer underlying the gabbroic base of the ophiolite, owing to the lack of discriminatory *S*-wave data, from mass balance calculations we favour a serpentinized mantle or mixed mantle and cumulate origin for this layer.

(ii) Several major normal faults downthrown to the west are interpreted from the model. These faults have throws of ∼500 m

offseting both the lava/dyke and dyke/gabbro boundaries and are interpreted to be syn-volcanic growth faults. No evidence is found for the existence of the previously proposed spreading centres at Larnaca and Mitsero. While the resolution of the models cannot exclude the existence of the Solea graben they do not appear to indicate a major bounding fault on the western side of the proposed graben. We propose that the geophysical data support a tectonic model incorporating a single spreading centre to the west of the ophiolite.

(iii) A deep reflector is imaged at ∼55 km depth beneath the ophiolite. This may originate from the northward subduction of the Sinai microplate beneath Cyprus.

ACKNOWLEDGMENTS

The IANGASS 1995 survey was undertaken with funding and support from the Department of Geology, University of Leicester, the Geological Survey Department of Cyprus and the Hellenic Mining company, Cyprus. Figures (with the exception of Fig. 1) were created using the GMT software of Wessel & Smith (1995). We would like to thank Simon Jowitt for the production of Fig. 1. We thank two anonymous reviewers for their comments which have improved the manuscript.

REFERENCES

Agar, S.M. & Klitgord, K.D., 1995. A mechanism for decoupling within the oceanic lithosphere revealed in the Troodos ophiolite, *Nature,* **374,** 232–238.

Allerton, S. & Vine, F.J., 1987. Spreading structure of the Troodos ophiolite, Cyprus: some paleomagnetic constraints, *Geology,* **15,** 593–597.

Allerton, S. & Vine, F.J., 1991. Spreading evolution of the Troodos ophiolite, Cyprus, *Geology,* **19**(6), 637–640.

Banks, G.J., 2004. Accretion of the lower oceanic crust in the Troodos ophiolite: textural and geochemical constraints from drill core CY-4, Cyprus, *Unpublished PhD thesis*, Cardiff University.

Baragar, W.R.A., Lambert, M.B., Baglow, N. & Gibson, I.L., 1990. Sheeted dykes from CY-4 and surface sections: Troodos ophiolite, in *Cyprus Crustal Study Project; initial report,* pp. 69–106, eds Gibson, I.L., Malpas, J., Robinson, P.T. & Xenophontos, C., Hole CY-4. Geological Survey of Canada.

Bartetzko, A., Delius, H. & Pechnig, R., 2005. Effect of compositional and structural variations on log responses of igneous and metamorphic rocks 1: mafic rocks, in *Petrophysical Properties of Crystalline Rocks,* Vol. 240, pp. 255–278, eds Harvey, P.K., Brewer, T.S., Pezard, P.A. & Petrov, V.A., Geological Society London, Special Publication.

Batanova, V.G. & Sobolev, A.V., 2000. Compositional heterogeneity in subduction related mantle peridotites, Troodos massif, Cyprus, *Geology,* **28**(1), 55–58.

Bear, L.M., 1960. The geology and mineral resources of the Akaki-Lythrodondha area, *Cyprus Geological Survey Memoir,* **3,** 122pp.

Ben-Avraham, Z., Tibor, G., Limonov, A.F., Leybov, M.B., Ivanov, M.K., Tokarev, M.Yu. &Woodside, J.M., 1995. Structure and tectonics of the eastern Cyprean arc, *Mar. Petrol. Geol.,* **12**(3), 263–271.

Bickle, M.J., Teagle, D.A.H., Beynon, J. & Chapman, H.J., 1998. The structure and controls on fluid-rock interactions in ocean ridge hydrothermal systems: constraints from the Troodoos ophiolite, in *Modern Ocean Floor Processes and the Geological Record,* pp. 127–152, eds Mills, R.A. & Harrison, K., Geological Society London, Special Publication.

Cann, J.R., 1970. New Model for the Structure of the Ocean Crust, *Nature,* **226**(5249), 928–930.

Cann, J.R., 1974. A model for oceanic crustal structure developed, *Geophys. J. R. Astron. Soc.,* **39**(1), 151–155.

Carlson, R.L., 1998. Seismic velocities in the uppermost oceanic crust; age dependence and the fate of layer 2A, *J. Geophys. Res.,* **103**(B4), 7069–7077.

Carlson, R.L. & Herrick, C.N., 1990. Densities and porosities in the oceanic crust and their variations with depth and age, *J. Geophys. Res.,* **95**(B6), 9153–9170.

Carlson, R.L. & Miller, D.J., 2004. Influence of pressure and mineralogy on seismic velocities in oceanic gabbros: implications for the composition and state of the lower crust, *J. Geophys. Res.,* **109,** B09205, doi:10.1029/2003JB002699.

Christensen, N.I. & Salisbury, M.H., 1975. Structure and constitution of the lower oceanic crust, *Rev. Geophys.,* **13,** 57–86.

Christensen, N.I., Wepfer, W.W. & Baud, R.D., 1989. Seismic properties of sheeted dikes from hole 504B, ODP Leg 111, in *Proceedings of the Ocean Drilling Programme, Scientific Results,* Vol. 111, pp. 171–176, eds Mazullo, E.K., Becker, K. *et al.,* Texas A&M University, Ocean Drilling Program, College Station, TX, USA.

Clube, T.M.M., Creer, K.M. & Robertson, A.H.F., 1985. Palaeorotation of the Troodos microplate, Cyprus, *Nature,* **317,** 522–525.

Collins, J.A., Brocher, T.M. & Purdy, G.M., 1989. Seismic-reflection structure of the upper oceanic crust: Implications from DSDP/ODP hole 504B, Panama Basin, in *Proceedings of the Ocean Drilling Programme, Scientific Results,* Vol. 111, pp. 177–191, eds Mazullo, E.K., Becker, K. *et al.,* Texas A&M University, Ocean Drilling Program, College Station, TX, USA.

Constantinou, G., 1995. *Geological map of Cyprus,* Geological Survey Department, Cyprus.

Coogan, L.A., Banks, G.J., Gillis, K.M., MacLeod, C.J. & Pearce, J.A., 2002. Hidden melting signatures recorded in the Troodos ophiolite plutonic suite: evidence for widespread generation of depleted melts and intracrustal melt aggregation, *Contribut. Mineral. Petrol.,* **144,** 485–505, doi 10.1007/s00410-002-0413-2.

Cooper, N.J., 1993. Integrated geophysical exploration of the north–east Troodos ophiolite, Cyprus, *Unpublished PhD thesis,* University of Leicester, p. 244.

Dercourt, J., Ricou, L.F. & Vrielynck, B. (eds), 1993. *Atlas of Tethys Palaeoenvironmental Maps,* Gauthier-Villars, Paris.

Detrick, R., Collins, J., Stephen, R. & Swift, S., 1994. In situ evidence for the nature of the seismic layer 2/3 boundary in oceanic crust, *Nature,* **370,** 288–290.

Ergün, M., Okay, S., Sari, C., Oral, Z.F., Ash, M., Hall, J. & Miller, H., 2005. Gravity anomalies of the Cyprus Arc and their tectonic implications, *Mar. Geol.,* **221,** 349–358.

Gass, I.G., 1960. The geology and mineral resources of the Dhali area. *Cyprus Geological Survey Department,* Memoir 4, 116pp.

Gass, I.G. & Masson-Smith, D., 1963. The geology and gravity anomalies of the Troodos massif, Cyprus, *Phil. Trans. R. Soc. Lond.,* **1060**(255), 417–467.

George, R.P. Jr., 1978. Structural petrology of the Olympus ultramafic complex in the Troodos ophiolite, Cyprus, *Geol. Soc. Am. Bull.,* **89,** 846–865.

Hagedoorn, J.G., 1959. The plus-minus method of interpreting seismic refraction sections, *Geophys. Prospect.,* **7,** 158–182.

Hurst, S.D, Moores, E.M. & Varga, R.J., 1994. Structural and geophysical expression of the Solea graben, Troodos ophiolite, Cyprus, *Tectonics,* **13**(1), 139–156.

Hyndman, R.D. & Peacock, S.M., 2003. Serpentinization of the forearc mantle, *Earth Planet. Sci. Letts.,* **212,** 417–432.

IAG (International Association of Geodesy) 1971. Geodetic Reference System 1967, IAG Publication Speciale No. 3 du Bulletin Geodesique.

Khan M.A., Summers, C., Bamford, S.A.D., Chroston, P.N., Poster, C.K. & Vine, F., 1972. Reversed seismic refraction line on the Troodos Massif, Cyprus, *Nature,* **238,** 134–136.

Kempler, D. & Ben-Avraham, Z., 1987. The tectonic evolution of the Cyprus arc *Ann. Tectonic,* **1,** 58–71.

Kidd, R.G.W. & Cann, J.R., 1974. Chilling statistics indicate an ocean-floor spreading origin for the Troodos Complex, Cyprus, *Earth Planet. Sci. Lett.,* **24,** 151–155.

Lort, J.M. & Matthews, D.H., 1972. Seismic velocities measured in rocks of the Troodos igneous complex, *Geophys. J. R. Astron. Soc.,* **27,** 383–392.

Makris, J., Ben-Avraham, Z.B., Behle, A., Ginzberg, A., Giese, P., Steinmetz, L., Whitmarsh, R.B. & Eleftheriou, S., 1983. Seismic refraction profiles between Cyprus and Israel and their interpretation, *Geophys. J. R. Astron. Soc.,* **75**(3), 575–592.

Mascle, J., Bellaiche, G., Loncke, L., Benkhelil, J., Zitter, T., Woodside, J. & Party, P.I.S., 2000. Marine geological evidence for a Levantine-Sinai plate, a new piece of the Mediteranean puzzle, *Geology,* **28**(9), 779–782.

Martinez, F. & Taylor, B., 2002. Mantle wedge control on back-arc crustal accretion, *Nature,* **416,** 417–420.

Muenow, D.W., Garcia, M.O., Aggrey, K.E., Bednarz, U. & Schmincke, H. U., 1990. Volatiles in submarine glasses as a discriminant of tectonic origin: application to the Troodos ophiolite, *Nature,* **343,** 159.

Miyashiro, A., 1973. The Troodos ophiolite was probably formed in an island arc, *Earth Planet. Sci. Lett.,* **19,** 218–224.

Moos, D., Goldberg, D., Hobart, M.A. & Anderson, R.N., 1986. Elastic wave velocities in Layer 2A from full waveform sonic logs at hole 504B, in *Initial Reports of the Deep Sea Drilling Project,* Vol. 92, pp. 563–570, eds Leinin, M. & Rea, D.K. *et al.,* US Government Printing Office, Washington, DC, USA.

Mukasa, S.B. & Ludden, J.N., 1987. Uranium-lead isotopic ages of plagiogranites from the Troodos ophiolite, Cyprus, and their tectonic significance, *Geology,* **15,** 825–828.

Osozawa, S. & Okamura, M., 1993. New radiolarian ages from the Troodos ophiolite and their tectonic implications, *Island Arc,* **2,** 1–6.

Payne, A.S. & Robertson, A.H.F., 1995. Neogene supra-subduction zone extension in the Polis graben system, west Cyprus, *J. Geol. Soc. Lond.,* **152,** 613–628.

Pedley, R.C., Busby, J.P. & Dabek, Z.K., 1993. GRAVMAG User Manual: Interactive 2.5D gravity and magnetic modelling, Technical Report WK/93/26/R, British Geological Survey.

Poole, A.J. & Robertson, A.H.F., 1992. Quarternary uplift and sea-level changes at an active plate boundary, Cyprus, *J. Geol. Soc. Lond.,* **148,** 909–921.

Robertson, A.H.F., 1998. Formation and destruction of the Eratosthenes seamount, Eastern Mediterranean Sea, and implications for collisional processes, in *Proceedings of the Ocean Drilling Program,* Vol. 160, pp. 681–699, eds Robertson, A.H.F., Emeis, K.-C., Richter, C. & Camerlenghi, A., Scientific Results.

Robertson, A.H.F. & Xenophontos, C., 1993. Development of concepts concerning the Troodos ophiolite and adjacent units in Cyprus, in *Magmatic Processes and Plate Tectonics,* Vol. 76, pp. 85–119, eds Prichard, H.M., Alabaster, T., Harris, N.B.W. & Neary, C.R., Geological Society London, Special Publication.

Salisbury, M.H., Christensen, N.I., Becker, K. & Moos, D., 1985. The velocity structure of Layer 2 at Deep Sea Drilling Project site 504 from logging and laboratory experiments, in *Initial Reports of the Deep Sea Drilling Project,* Vol. 83, pp. 529–539, Anderson, R.N. *et al.,* US Government Printing Office, Washington, DC, USA.

Salisbury, M.H., Christensen, N.I., Vine, F.J., Smith, G.C. & Eleftheriou, S., 1989. Geophysical structure of the Troodos ophiolite from downhole logging, in *Cyprus Crustal Study Project: Initial report,* pp. 331–349, eds Gibson, I.L., Malpas, J., Robinson, P.T. & Xenophontos, C., Hole CY-4, Geological Society of Canada, 88-9.

Schouten, H. & Denham, C.R., 2000. Comparison of volcanic construction in the Troodos ophiolite and oceanic crust using paleomagnetic inclinations from Cyprus Crustal Study Project (CCSP) CY-1 and CY-1A and Ocean Drilling Program (ODP) Hole 504B drill cores, in *Geological Society of America Special paper,* Vol. 349, pp. 181–194, eds Dilek, Y., Moores, E., Elthon, D. & Nicolas, A.

Shelton, A.W., 1993. Troodos revisited: The Mount Olympus gravity anomaly, in *Magmatic Processes and Plate Tectonics,* Vol. 76, pp. 197–212, Prichard, H.M., Alabaster, T., Harris, N.B.W. & Neary, C.R., Geological Society London, Special Publication.

Smith, G.C. & Vine, F.J., 1987. Seismic velocities in basalts from C.C.S.P. drill hole CY-2 and CY-2a at Agrokipia Mines, Cyprus, in *Cyprus Crustal Study Project: Initial report, holes CY-2 and 2a,* pp. 295–306, eds Robinson, P.T., Gibson, I.L. & Panayiotou, A., Geological Society of Canada, 85–29.

Smith, G.C. & Vine, F.J., 1989. The physical properties of diabases, gabbros and ultramafic rocks from C.C.S.P drill hole CY-4 at Palekhori, Cyprus, in *Cyprus Crustal Study Project: Initial report, holes CY-4,* pp. 295–314, eds Robinson, P.T., Gibson, I.L. & Panayiotou, A., Geological Society of Canada, 88-9.

Smith, G.C. & Vine, F.J., 1991. The physical properties of basalts from C.C.S.P. drill holes CY-1 and CY-1a, Akakai Canyon, Cyprus, in *Cyprus Crustal Study Project: Initial report, holes CY-1 and 1a,* pp. 217–234, eds Robinson, P.T., Gibson, I.L. & Panayiotou, A., Geological Society of Canada, 90-20.

Stephen, R.A., 1988. Lateral heterogeneity in the upper oceanic crust at deep sea drilling project site 504, *J. Geophys. Res.,* **93**(B6), 6571–6584.

Sun, Y-F. & Goldberg, D., 2000. Characterization of the upper oceanic crust using high-resolution seismic amplitude modeling, in *Ophiolites and Oceanic Crust: New insights from field studies an the Ocean Drilling,* Vol. 349, pp. 203–210, eds Dilek, Y., Moores, E.M., Elthon, D. & Nicholas, A., Program. Geol. Soc. Am. Spec. Paper.

Swain, C.J. & Khan, M.A., 1977. A catalogue of gravity measurements in Kenya, *Unpublished report, Department of Geology,* University of Leicester.

Swift, S.A., Lizarralde, D., Stephen, R.A. & Hoskins, H., 1998. Velocity structure in upper ocean crust at Hole 504B from vertical seismic profiles. *J. Geophys. Res.,* **103**(B7), 15 361–15 376.

Swift, S.A. & Stephen, R.A., 1989. Lateral heterogeneity in the seismic structure of oceanic crust, western North Atlantic, *J. Geophys. Res.,* **94**(B7), 9303–9322.

Taylor, R.N., 1983. The stratigraphy, geochemistry and petrogenesis of the Troodos extrusive sequence, Cyprus. *Unpublished PhD Thesis, University of Southampton*.

Van Everdingen, D.A. & Cawood, P.A., 1995. Dyke domains in the Mitsero graben, Troodos ophiolite, Cyprus: an off-axis model for graben formation at a spreading centre, *J. Geol. Soc. Lond.,* **152,** 923–932.

Varga, R.J. & Moores, E.M., 1985. Spreading structure of the Troodos ophiolite, Cyprus, *Geology,* **13,** 846–850.

Varga, R.J., Gee, J.S., Bettison-Varga, L., Anderson, R.S. & Johnson, C.L., 1999. Early establishment of seafloor hydrothermal systems during structural extension: paleomagnetic evidence from the Troodos ophiolite. *Earth Planet. Sci. Lett.,* **171,** 221–235.

Wessel, P. & Smith, W.H.F., 1995. New version of the Generic Mapping Tools released, *EOS, Trans. Am. Geophys. Un.,* **76,** 329.

White, R.S. & Whitmarsh, R.B., 1984. An investigation of seismic anisotropy due to cracks in upper oceanic crust at 45°N, Mid-Atlantic Ridge, *Geophys. J. Int.,* **79,** 439–467.

Wilkins, R.H. & Langseth, M.G., 1983. Physical properties of sediments of the Costa Rica Rift, Deep Sea Drilling Project sites 504 and 505, *Initial Rep. Deep Sea Drill Project,* **69,** 659–674.

Wilson, D.S. *et al.*, 2006. Drilling to gabbro in intact oceanic crust, *Science,* **312,** 1016–1020.

Wilson, R.A.M., 1959. The geology of the Xeros-Troodos area, *Cyprus Geological Survey Department,* Memoir 1, 135pp.

Zelt, C.A., 1999. Modelling strategies and model assessment for wide-angle seismic traveltime data, *Geophys. J. Int.,* **139,** 183–204.

Zelt, C.A. & Barton, P.J., 1998. Three-dimensional seismic refraction tomography: A comparison of two methods applied to data from the Faeroe Basin, *J. Geophys. Res.,* **103**(B4), 7187–7210.

Zelt, C.A. & Forsyth, D.A., 1994. Modeling of wide-angle seismic data for crustal structure: Southeastern Grenville Province, *J. Geophys. Res.,* **99**(B6), 11 687–11 704.

Zelt, C.A. & Smith, R.B., 1992. Seismic traveltime inversion for 2-D crustal velocity structure, *Geophys. J. Int.,* **108,** 16–34.